AD_____

Award Number: DAMD17-02-1-0719

TITLE: Interrogating Androgen Receptor Mediated Gene Expression and Tumor Progression by Molecular Imaging

PRINCIPAL INVESTIGATOR: Michael F. Carey, Ph.D.

CONTRACTING ORGANIZATION: University of California, Los Angeles
Los Angeles, CA 90024-1406

REPORT DATE: October 2005

TYPE OF REPORT: Final

PREPARED FOR: U.S. Army Medical Research and Materiel Command
Fort Detrick, Maryland 21702-5012

DISTRIBUTION STATEMENT: Approved for Public Release;
Distribution Unlimited

REPORT DOCUMENTATION PAGE

Form Approved
OMB No. 0704-0188

1. REPORT DATE *(DD-MM-YYYY)*	2. REPORT TYPE	3. DATES COVERED *(From - To)*
01-10-2005	Final	9 Sep 2002 – 8 Sep 2005

4. TITLE AND SUBTITLE
Interrogating Androgen Receptor Mediated Gene Expression and Tumor Progression by Molecular Imaging

5a. CONTRACT NUMBER

5b. GRANT NUMBER
DAMD17-02-1-0719

5c. PROGRAM ELEMENT NUMBER

6. AUTHOR(S)
Michael F. Carey, Ph.D.

E-mail: mcarey@mednet.ucla.edu

5d. PROJECT NUMBER

5e. TASK NUMBER

5f. WORK UNIT NUMBER

7. PERFORMING ORGANIZATION NAME(S) AND ADDRESS(ES)
University of California, Los Angeles
Los Angeles, CA 90024-1406

8. PERFORMING ORGANIZATION REPORT NUMBER

9. SPONSORING / MONITORING AGENCY NAME(S) AND ADDRESS(ES)
U.S. Army Medical Research and Materiel Command
Fort Detrick, Maryland 21702-5012

10. SPONSOR/MONITOR'S ACRONYM(S)

11. SPONSOR/MONITOR'S REPORT NUMBER(S)

12. DISTRIBUTION / AVAILABILITY STATEMENT
Approved for Public Release; Distribution Unlimited

13. SUPPLEMENTARY NOTES

14. ABSTRACT
This final report summarizes our work on the effectiveness of a new adenovirus based optical imaging vector designed to detect MAP kinase levels in living subjects. The vector was injected into human tumors implanted into SCID mice. Animals were injected with D-luciferin and imaged in a Xenogen IVIS device. The vector was able to detect enhanced MAPK levels stimulated by Epidermal Growth Factor in prostate cancer tumors of xenograft animals. We interrogated two lines of androgen dependent (AD) and independent (AI) xenograft animal models (CWR22 and LAPC9) to determine MAPK levels. We found no significant difference between AD and AI cancer with respect to functional MAPK levels. However, CWR22 animals exhibit significantly higher MAPK levels than LAPC9 xenograft animals. The data suggest the possibility that gene expression based imaging may be able to detect augmented MAPK levels predictive of disease progression as well as the efficacy of cancer therapeutics.

15. SUBJECT TERMS
No subject terms provided.

16. SECURITY CLASSIFICATION OF:			17. LIMITATION OF ABSTRACT	18. NUMBER OF PAGES	19a. NAME OF RESPONSIBLE PERSON
a. REPORT	b. ABSTRACT	c. THIS PAGE			USAMRMC
U	U	U	UU	74	19b. TELEPHONE NUMBER *(include area code)*

Table of Contents

Introduction: The goal of our DOD-funded project was to analyze the mechanism of androgen-receptor (AR)-mediated gene activation in androgen-independent (AI) xenograft models of prostate cancer using powerful new technologies: Noninvasive optical imaging, chromatin immunoprecipitation and immobilized template analysis. Our previous studies have demonstrated our ability to track metastatic lesions and illuminate prostate cancer using gene expression-based imaging cassettes in combination with a charge coupled device (CCD) optical imaging system. Our imaging cassette is termed TSTA or two-step transcriptional activation. In TSTA, a modified PSA enhancer is employed to synthesize GAL4-VP16, which activates luciferase expression to very high levels. This strategy effectively maintains the tissue and signal specificity but amplifies the transcriptional output and Luciferase levels of weak cellular promoters allowing us to visualize their action in dense tissues like xenograft tumors. A current hypothesis in the field is that elevated mitogen activated protein kinase (MAPK) activity, initiated by receptor tyrosine kinase (RTK) signaling (Figure 1), plays a role in AI prostate cancer. This directly or indirectly leads to augmented transcription complex assembly and expression of AR-regulated genes *in vivo*. The mechanism of this effect is largely unknown but may influence the development of AI cancer. The working hypothesis is that MAPK signaling induces modifications of AR function that permit AR to act in a ligand-depleted environment. Our goal was to develop a prostate cancer imaging system to detect augmented MAPK activity in prostate tumors implanted into living animals and correlate it with enhanced AR function.

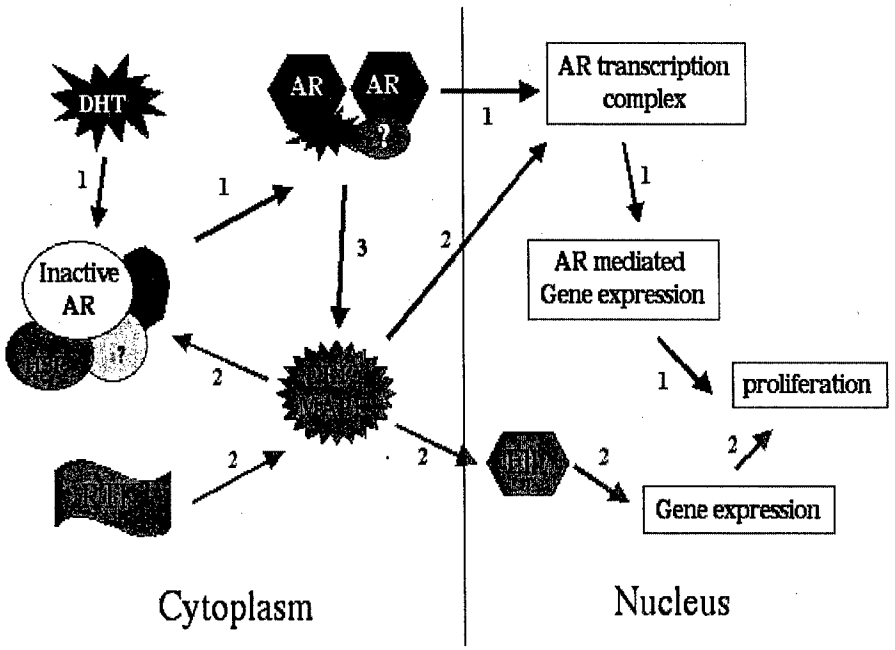

Figure 1 AR-mediated prostate cancer growth: A diagram of proposed mechanisms for AR-regulated gene expression and cell growth. In pathway 1, DHT binds AR, causing dissociation of HSP chaperones, dimerization, nuclear localization, transcription complex assembly, gene activation and cell proliferation. In pathway 2, Receptor tyrosine kinase (RTK)-linked MAPK cascades converge at ERK, which activates Elk-1 and possibly some components of the AR transcription complex. This allows growth of prostate cancer at castrate levels of ligand. An alternative pathway is that MAPKs facilitate response to castrate levels of ligand by acting on the chaperone complex and the nuclear localization of AR. Finally, pathway 3 illustrates a non-genotropic mechanism by which AR activates the MAPK pathway directly

Statement of Work and Results

Task 1: Develop the MAPK-TSTA expression system.

The initial goal of the study was to develop an imaging system that could detect elevated MAPK levels during the transition between the androgen dependent (AD) and independent (AI) forms of prostate cancer in xenograft animal models. The basic hypothesis as stated in Figure 1 is that elevated MAPK facilitates the conversion to the AI state. To test the idea that MAPK is elevated in AI xenografts we developed a plasmid-based imaging system founded on a concept of TSTA.

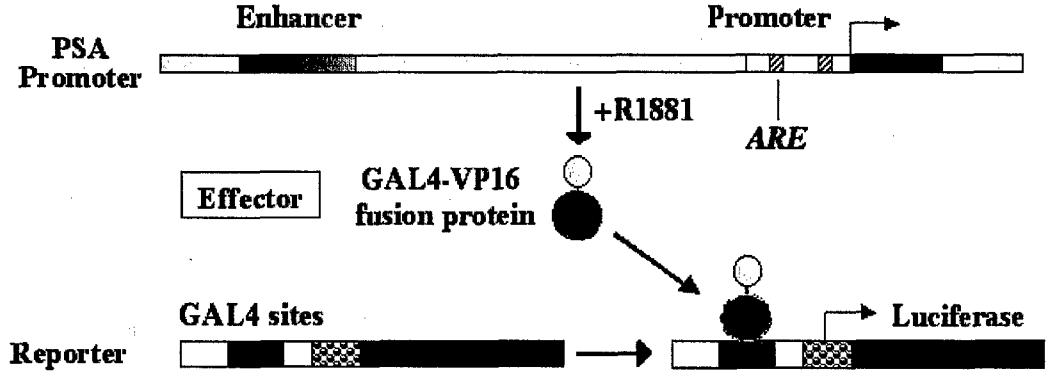

Figure 2. The Rationale of Two Step Transcription Activation (TSTA) system. In the first step, the "effector" GAL4-VP16 derivatives (oval circles) are expressed in prostate cancer cells in the presence of androgen (R1881), which activates the PSA enhancer, PSE. In the second step, GAL4-VP16 binds to a GAL4-responsive promoter, and activates expression of the "reporter" firefly luciferase. GAL4: GAL4 DNA Binding Domain. VP16: VP16 activation domain. E4TATA contains the adenovirus E4

In the TSTA system (Figure 2) a prostate specific, androgen receptor (AR)-responsive prostate specific antigen (PSA) enhancer drives GAL4-VP16. GAL4-VP16 is a potent transcriptional activator and binds to GAL4 recognition sites upstream of a Firefly luciferase reporter gene. When AR is active then GAL4-VP16 is synthesized, binds DNA, and luciferase is expressed. The amount of luciferase is proportional to the amount of AR activity in the cell. We measure luciferase in cell culture by adding D-luciferin and ATP to cell extracts and light is quantitated using standard luminometry. In live animals, we inject D-luciferin into the animal and detect luciferase activity using a Xenogen charge coupled device camera, which quantifies the photons emitted from tissues expressing luciferase in the live animal. The process is not toxic and animals can be imaged repetitively over weeks or months. The system is described in several previous publications from my lab with my collaborators, Drs. Sam Gambhir and Lily Wu. These are listed under Reportables below.

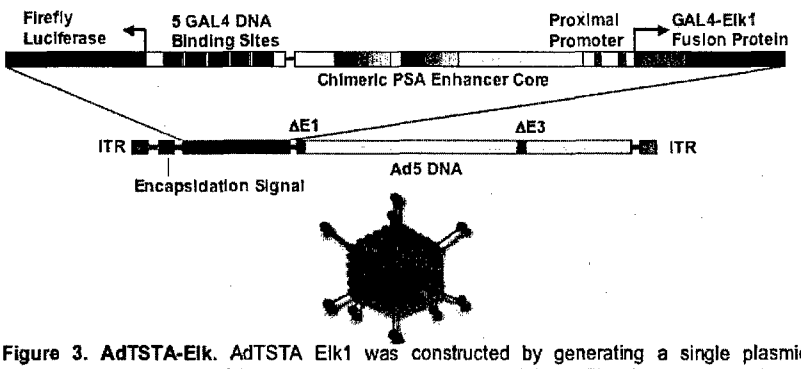

Figure 3. AdTSTA-Elk. AdTSTA Elk1 was constructed by generating a single plasmid containing the chimeric PSA enhancer driving expression of GAL4-Elk1 fusion protein. In the presence of active androgen receptor GAL4-Elk1 is synthesized and binds to the 5 GAL4 sites upstream of the firefly luciferase reporter gene. GAL4-Elk1 is inactive however until it is phosphorylated by active MAPK (ERK1 and 2). Thus, as described in our proposal, the system will only synthesize luciferase in prostate tissue, when AR is active and when MAPK levels are elevated. The TSTA-Elk1 cassette was cloned into pShuttle and recombined into the adenovirus genome in bacteria using AdEASY. Genomic DNA was isolated and transfected into 293A cells. The virus was plaque purified, scaled up and used for injection studies into LAPC9 xenografts in SCID mice.

After having established the activity of AR in the original transcription based TSTA imaging system we next modified TSTA to measure MAPK activity. We took advantage of the fact that MAPK activates the transcription factor ELK-1 by phosphorylation as stated in Figure 1. We replaced the VP16 activation domain in our TSTA cloning vectors with that of ELK-1. In year 1 we reported the successful outcome of initial cell culture tests. These data are shown in the attached submitted paper (Ilagan et al). In year 2, the single plasmid TSTA-ELK system was cloned into an adenovirus shuttle vector. We isolated individual plaques and purified the virus. Figure 3 shows a schematic of the final viral construct and describes the steps in its synthesis. In year 3 we performed extensive experiments comparing the MAPK levels in AD and AI tumors. These data will be described below.

Task 2: Testing the TSTA-ELK system in cell based assays.

The goal of this task was to test for prostate specificity of the TSTA-ELK system in cell lines and to test for response to androgens, MAPK stimuli and pathway inhibitors. This phase of the testing was completed in years 1 and 2. Two figures are included below showing 1. The response of TSTA-ELK plasmids in LNCaP cells to co-transfected plasmid expressing DA-MEKK, an upstream activator of MEK and ERK1/2 (Figure 4); 2. The response of TSTA-ELK to EGF an activator of the ERK1/2 pathway (Figure 5). In both cases the reporter response to

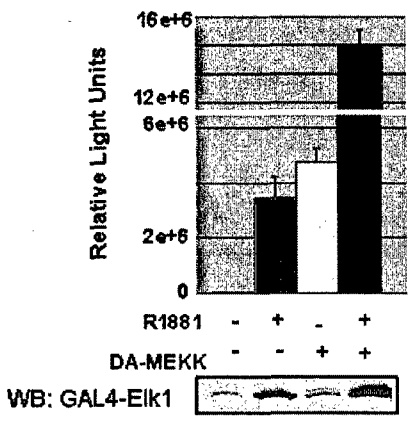

Figure 4. The TSTA-ELK1 Prostate and MAPK Specific Imaging Construct. Validation of TSTA-ELK1 response to AR and MAPK pathways in cultured cells. LNCaP prostate cancer cells grown in 6-well plates were transiently transfected with TSTA-ELK1 plasmid. We added 10 nM R1881 (synthetic androgen) and dominant active MEKK (DA-MEKK), together or separately, to samples 1 hour after transfection and measured the luciferase activity 48 hours after stimulation. These experiments were repeated multiple times in triplicate. The measurements shown here are average values of a representative experiment. The vertical axis shows the relative light units (RLuc) reading from the luminometer. The error bars represent standard deviation (STD). Below the graph is an immunoblot showing LNCaP cell extracts probed with GAL4 antibodies to detect GAL4-ELK1 expression.

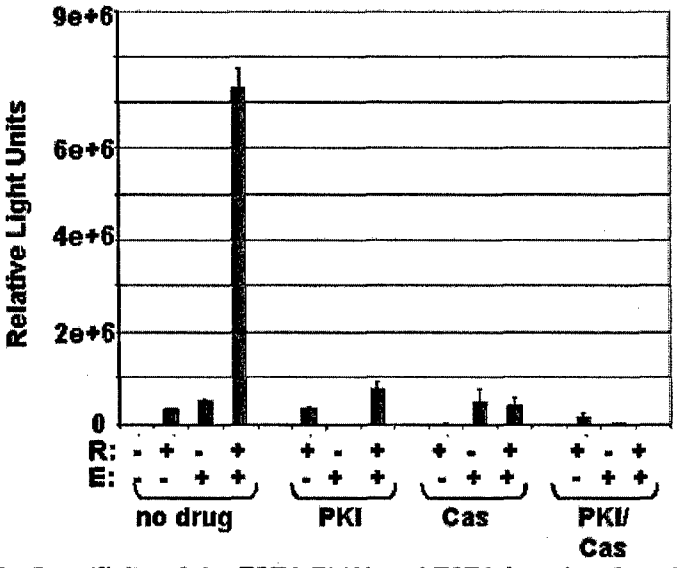

Figure 5. Specificity of the TSTA-ELK1 and TSTA Imaging Constructs. FLuc assay of LNPCaP cells transiently transfected with TSTA-ELK1 plasmid. Cells were treated together or separately with 0.1 nM R1881 and 100 ng of recombinant epidermal growth factor (EGF) and with or without inhibitors PKI-166 (PKI) a RTK inhibitor of the MAPK cascade and casodex (Cas) an anti-androgen. Cell lysates were assayed for FLuc activity 48 hours after treatment using a luminometer. Assays were done in triplicate and representative FLuc assay is shown.

the combined action of the MAPK stimulant and androgen (R1881) was synergistic. Additionally the system was able to detect the effect of EGFR and AR inhibitors, PKI and Flutamide, respectively. The data were accumulated in years 1 and 2 and set the stage for the in vivo studies.

Task 3: Testing the MAPK-TSTA system in live animals.

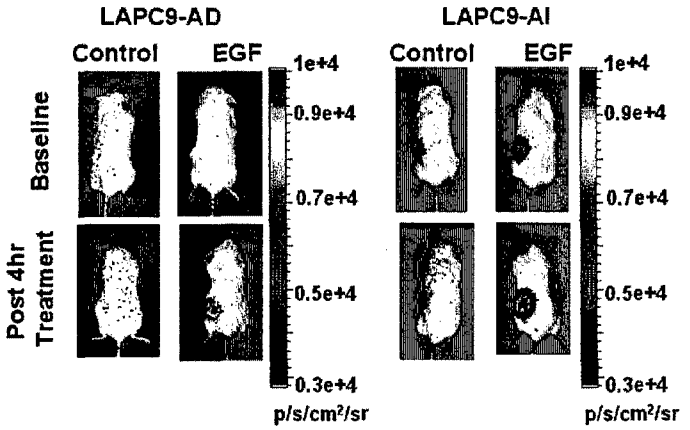

Figure 6. Imaging AR and MAPK signaling in the LAPC9 prostate cancer xenograft model. Castrated (AI) or intact (AD) male SCID mice implanted subcutaneous with LAPC9 tumors (0.5cm) and were injected intratumorally with 2e+7 pfus of AdTSTA-ELK1. After 3 days mice were injected intraperitoneally with of EGF or vehicle control and then imaged 4 hours later to evaluate MAPK activation. Representative mice are shown post 4 hours EGF treatment from the LAPC9-AD group (n=8) and LAPC9-AI group (n=8).

The goal of task 3 was to generate systems that could detect elevated MAPK signaling in prostate tumors using gene expression-based optical imaging. My student Ms. Myla Ilagan and my technician Ms. Jill Pottratz generated a TSTA-ELK1 adenovirus (AdTSTA-ELK1) expressing firefly luciferase (Figure 3). Our cell culture data from years 1 and 2 suggested that TSTA-ELK1 could

image MAPK activity in a tumor. The data above are the first example of gene expression-based imaging of MAPK in xenograft tumors and are reported in Ms. Ilagan's submitted manuscript.

Previous studies have shown that EGF activates MAPK levels in LAPC9 tumors implanted into SCID mice. Figure 6 shows a representative experiment demonstrating the ability of the virus to respond to EGF, a known MAPK stimulant, in the context of LAPC9 AD and AI tumors. The data for cohorts of 8 AD and AI animals are graphed in Figure 7. The experiment established proof of principle that we can measure MAPK activity in live animals using gene expression cassettes coupled with optical imaging technologies.

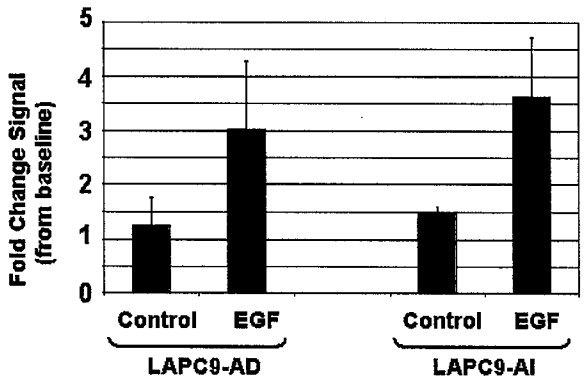

Figure 7. Bar graph summarizing several experiments with cohorts of n=8 of LAPC9-AD and LAPC9-AI xenografts injected with AdTSTA-ELK1. Graph depicts the fold change of signal of AdTSTA-ELK1 activity post-EGF treatment. Error bars indicate standard deviation.

Task 4: Analyze the AR-MAPK pathway using the TSTA-ELK1 *in vivo* imaging system.

After completion of this proof of principle experiment we began to analyze the basal MAPK levels in two xenograft models of cancer, LAPC9 and CWR22. We also evaluated the effects of drugs on the AR and MAPK signaling pathways.

Figure 8 shows the optical CCD signals from representative AD and AI animals 3 days after viral injection. We illustrate the animals using the same photonic scale to show the large difference between models as described below. Figure 9 graphs a representative experiment performed with cohorts (n=10 for AD and n=8 for AI) of animals. Two important observations emerged from this analysis. First, we found only marginal differences between the AD and AI tumors within each xenograft model. This suggests that MAPK levels do not change significantly when the tumor transitions into the AI state in the xenografts. The second observation was that the AdTSTA-ELK1 activity in the CWR22 models is over 100-fold higher than the signal observed in the LAPC9 models (Figure 9). This latter

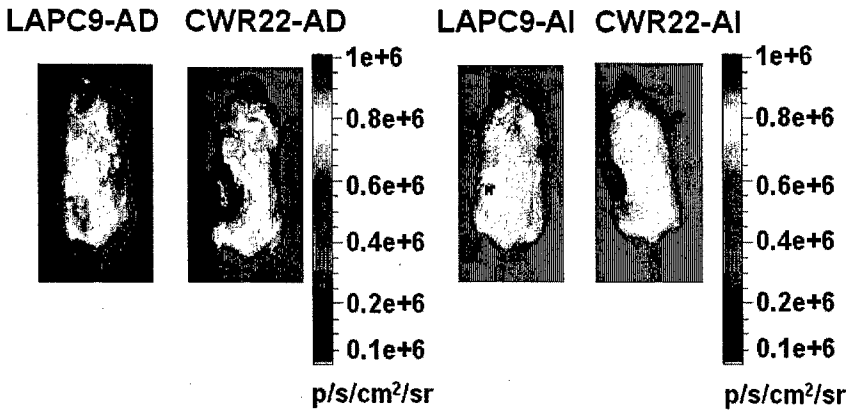

Figure 8. Comparison of the Basal Activities of LAPC9 and CWR22 Xenografts. LAPC9 (AD, AI) and CWR22 (AD, AI) xenografts were injected intratumorally with 4.7e+07 pfus of AdTSTA-ELK1. Pseudoimages were normalized to the CWR22 xenograft images to demonstrate the difference in signals between the two prostate cancer xenografts.

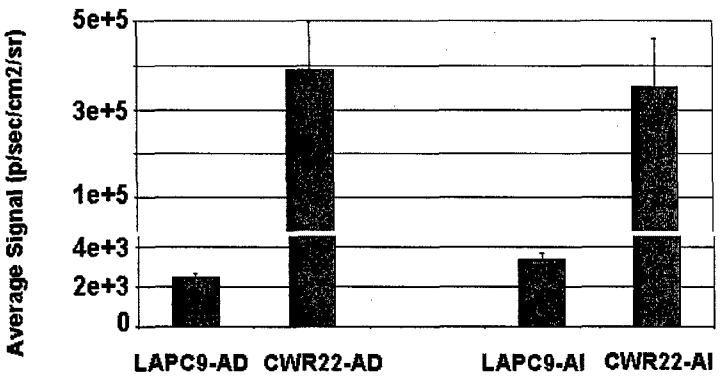

Figure 9. Bar graph summarizing the average basal signal of the two prostate cancer xenografts in photons/second/cm²/steridian. Graph depicts the average basal level signals on day 3 following injection of virus.

observation suggested the possibility that the xenograft models display vastly different levels of functional MAPK. This explanation, however, required further validation as it could imply that elevated MAPK is not a common feature of advanced or recurrent PCa cancer in xenografts.

We considered the possibility that the CWR22 AD and AI tumors grew at a significantly different rate versus LAPC9. MAPK levels are known to be elevated in highly proliferating cells. We measured the increase in tumor volume (in cm^3) over time as the tumors began to proliferate from palpable to measurable sizes. We found that although the CWR22 AI tumors displayed the fastest rate of growth, the second fastest were the LAPC9 AI followed by the CWR22 AD and then the LAPC9 AD. Thus, there is no correlation between functional MAPK and the growth rates of the different xenografts.

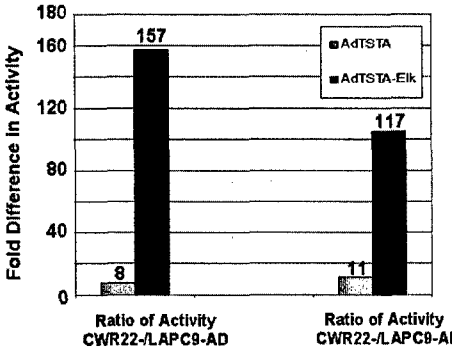

Figure 10. Comparing the MAPK Specificity of AdTSTA-ELK1 and AdTSTA in the LAPC9 and CWR22 Xenograft Models. AdTSTA-ELK1 and AdTSTA were injected into LAPC9 or CWR22 xenografts when tumors reached <0.5 cm in diameter. Baseline signals of each imaging construct were taken after 3 days post injection of the viral vector. Graph depicts the fold difference in activity of each imaging construct in the each xenograft model (LAPC9 vs. CWR22) and each model type (AD vs. AI). AdTSTA-ELK1 shows greater fold activity (157) in signal between LAPC9- and CWR22-AD models and similarly (117-fold) with LAPC9- and CWR22-AI models.

Another possibility was that the differences in AdTSTA-ELK1 activity derive from differences in the functional AR activity or infectivity of the adenovirus in the different xenograft models. To address these issues we injected cohorts of LAPC9 and CWR22 AD and AI xenografts with low levels of AdTSTA. As described above, AdTSTA expresses GAL4-VP16 from a modified PSA enhancer and measures the AR responsiveness of a prostate tumor. The bar graph in Figure 10 compares the ratio of the AdTSTA activity in LAPC9 versus CWR22 AD and AI tumors against the AdTSTA-ELK1 activities. The data show that CWR22 xenografts do display higher functional AR activity. The differences average 8 fold for the AD xenografts and 11 fold for the AI xenografts. However, when the AdTSTA-ELK1 ratios are compared there is a 157-fold difference between the CWR22 and LAPC9 AD xenografts and a 117-fold difference between the AI xenografts. After dividing the AdTSTA-ELK1 differences by the AdTSTA values there is a 20-fold difference between the AdTSTA-ELK1 and AdTSTA activity in AD tumors and a 10-fold difference in AI tumors that cannot be

accounted for on the basis of AR activity or differential infectivity. We suggest that this difference is due to the basal MAPK activity existing in the xenografts.

To further understand the consequences of the enhanced functional MAPK levels we performed immunoblotting analysis of the tumors from sacrificed animals as shown in Figure 11. We prepared tumor extracts by mincing the tissue and heating in SDS-containing buffer followed by immunoblot using antibodies to AR, PSA, ERK, phospho-ERK and β-actin. We carefully normalized the protein levels in each extract using protein assays and Coomassie stained SDS-gels. We further normalized the loading to the overall β-actin and ERK levels of the tumor. We chose to show two representative samples from the CWR22 and LAPC9 AD and AI models although they are highly representative of over a dozen different independent tumor isolates. The data were analyzed by laser densitometry.

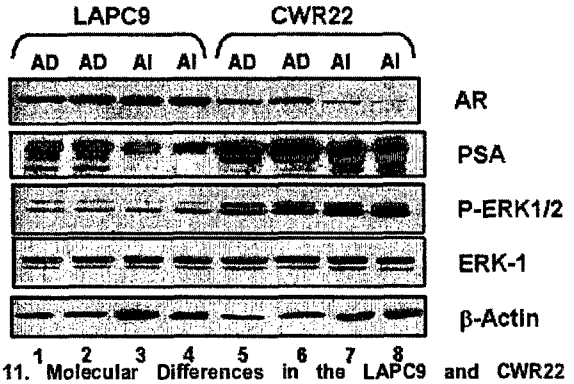

Figure 11. Molecular Differences in the LAPC9 and CWR22 Xenograft Models. Western blot analysis AR, PSA, ERK1/2 (p42/44) and ERK1 (p44) expression from harvested and extracted xenografts. Total proteins were extracted from tumors and immunoblotting was performed using specific antibodies against each protein. β-actin and ERK were used to normalize loading of the extracts onto the gels for the final immunoblot. Lanes 1, 2, 5 and 6 depict independent isolates of androgen dependent (AD) tumor samples from LAPC9 (lanes 1 and 2) and CWR22 tumors (lanes 5 and 6). Lanes 3, 4, 7, and 8 depict separate androgen independent (AI) tumor samples from LAPC9 (lanes 3 and 4) and CWR22 (lanes 7 and 8) tumors.

There are several important observations that bear mentioning. The overall ERK levels are similar between the LAPC9 and CWR22 AD and AI xenografts when normalized to protein concentration in the tumor extracts. However, phospho-ERK levels are on average 6-fold higher in CWR22 versus the LAPC9 models. Thus we surmise that the enhanced AdTSTA-ELK1 imaging activity is due in part to enhanced phospho-MAPK environment in the xenografts.

Surprisingly, the PSA levels between the xenografts also varied. The levels in CWR22 tumors AD and AI were similar but approximately 3.4 and 4.6 fold higher respectively, than their LAPC9 counterparts. This latter observation correlates roughly with the AdTSTA imaging data, where the differences were 11 and 8 fold. Thus, it is likely that the differences between the CWR and LAPC9 xenografts represent a combination of both increased AR and MAPK function.

Remarkably, the AR levels in the xenografts were also different. LAPC9 AD and AI tumors displayed approximately equal levels of AR but they were 1.5 fold higher than those found in the CWR22 AD model. Equally surprising was the finding that CWR22 AD tumors displayed significantly higher levels than AI tumors. Although AR and MAPK are proposed to be central molecules in PCa growth, we found no tight correlation between either or between PSA expression and tumor growth rate. Taken together with the imaging data our study suggests some surprising properties of PCa xenografts that illustrate the heterogeneity of different tumors.

Our most recent studies focused on evaluating the effects of Flutamide, an AR inhibitor, and Iressa, an EGF receptor tyrosine kinase inhibitor, using the AdTSTA and ADTSTA-ELK systems. The goal was to determine if the systems could accurately

measure inhibition of signaling in tumors of live animals. We began by analyzing a drug known to inhibit AR function. Because our previous study showed that AdTSTA accurately measured AR signaling in xenografts we felt it was a solid starting point in our quest to develop imaging tools that could be used in drug testing and development. In our Molecular Cancer Therapeutics paper (in press) adenoviruses bearing an optical imaging cassette containing an AR-responsive two-step transcriptional amplification system (AdTSTA) were injected into LAPC9 AD and AI tumors of animals undergoing systemic time controlled release of the anti-androgen flutamide. Imaging revealed that the response of AdTSTA to flutamide is more sensitive and robust than serum PSA measurements. Figure 12 shows that flutamide inhibits the androgen-signaling pathway in androgen-dependent but not refractory tumors. Additionally we performed an analysis of AR and RNA polymerase II binding to the endogenous PSA gene by chromatin immunoprecipitation within the tumors. Unlike the effect of androgen deprivation reported in Zhang et al (2003), flutamide does not inhibit AR nuclear localization or binding to the PSA enhancer in AD tumors. This demonstrates that flutamide treatment and androgen withdrawal have different molecular mechanisms.

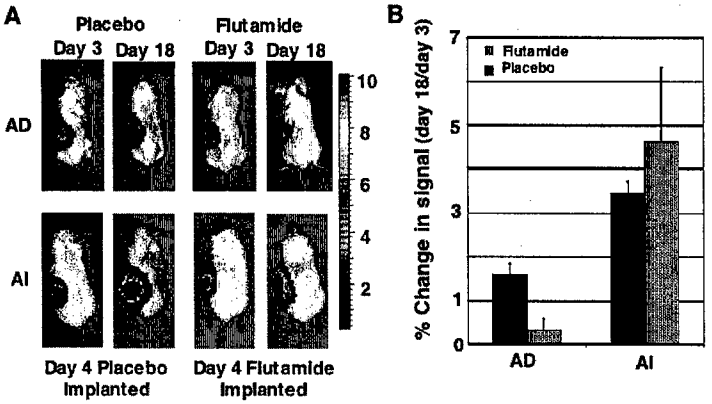

Figure 12. LAPC9 AI Tumors Are Resistant to Flutamide. AdTSTA were injected intratumorally into intact (AD) or castrated (AI) male mice bearing LAPC9 xenografts. A. Typical effects. On day 3 a baseline image was acquired and flutamide or placebo pellets were implanted. The effect of treatment at day 18 is shown. We have not detected any flutamide effect in the LAPC9 AI tumor model. B. Cohorts. Cohorts of n=7 AD and n=6 AI animals were studied. The data are graphed as the percent change in signal versus day 3 in placebo and flutamide treated animals bearing AD and AI tumors.

In our original DOD proposal we proposed to use the EGFR/HER2 inhibitor PKI-166 in our MAPK studies based on a report from my colleague Charles Sawyers lab. We were however not able to obtain growth inhibition of LAPC9 tumors as his lab reported and the amount of drug available was low. We therefore began testing the effect of Iressa on growth of CWR22 and LAPC9 AI tumors to study its efficacy. Iressa is an EGFR inhibitor and we had two collaborators who were experienced in large-scale preclinical studies and who would make large quantities of drug available. We performed six studies that are summarized below; the imaging and tumor data were analyzed by Student's T-test as described in the appended publications.

In collaboration with the David Agus lab at Cedars-Sinai Hospital in Los Angeles we performed three studies on the effect of Iressa on LAPC9-AI animals using daily doses of 150mg/kg administered orally. Study A) 4=Iressa, 3=vehicle; Study B) 5=Iressa, 5=vehicle; Study C) 4=Iressa, 5=vehicle. In all three studies we failed to see any effect of Iressa on AdTSTA-ELK activity and tumor growth, and we did not see a diminution in Phospho-Erk levels when animals were sacrificed and tumors were analyzed by immunoblotting.

In collaboration with the Dennis Slamon lab at UCLA we performed three studies with the CWR22-25/24 (AI) model. Study A) 7=Iressa, 6=vehicle at an Iressa dose of150mg/kg. We observed a statistically significant tumor growth inhibition in this study

but there was no decrease in AdTSTA-ELK activity or in Phospho-Erk levels as analyzed by immunoblotting. However the Iressa treated mice demonstrated some symptoms of toxicity including grooming defects and weight loss. In study B), 5=Iressa, 4=vehicle, we tried a lower dose of Iressa 100mg/kg because of concerns about toxicity in mice. We observed no decrease in tumor growth or in AdTSTA-ELK activity. Because the higher dose seemed to have an effect in study A we performed a short-term study again at the higher dose, while carefully monitoring animal health. Study C), 10=Iressa, 10=vehicle, employed Iressa at a dose of 150mg/kg. This study did not show the significant and sustained inhibition in tumor growth as seen in study A. We did observe a small but significant difference ($p=0.009$) in tumor size on day 8 in Iressa versus vehicle treated animals but poor animal health proscribed us from analyzing this further and the mice were sacrificed. Additionally, there was no significant difference in AdTSTA-ELK activity. It is plausible that at the high drug combinations Iressa is inhibiting a pathway other than that controlled by EGFR and that the weak and sporadic effects of Iressa are due to an off-target inhibitory effect. Overall, the data show that Iressa is not inhibiting tumor growth and suggest that EGFR and MAPK are not driving tumor growth in the LAPC9 and CWR22 AI models.

Task 5: Perform nuclear localization tests of AR

One of the key questions regarding AR function during androgen independent prostate cancer is whether it has the ability to localize the nucleus in the presence of castrate levels of ligand. AR is in the nucleus of LAPC9 AI tumors a reported in Zhang et al. 2003.

Task 6: Perform chromatin immunoprecipitation on AD and AI tumors.

We found that AR and pol II bound to promoters of the PSA gene in AI tumors. The data are published in Zhang et al. 2003.

Task 7: Perform immobilized template assay.

Our attempts to employ the immobilized template in crude tumor extracts have been unsuccessful. These extracts are significantly more proteolyzed than ones from cell culture and contain significant hemoglobin due to contamination with blood from the animal. While we continue to be interested in performing this experiment it is not technically feasible.

Key Research Accomplishments 2002-2005:

- Demonstration that AR is fully active in AI xenografts as measured by AdTSTA activity.
- Demonstration that AR is fully active in AI cancer as measured by nuclear localization and ChIP on the PSA regulatory region.
- Demonstration that AdTSTA can detect the effect of small molecule pharmaceuticals on AR signaling and tumor growth in LAPC9 xenografts.
- Creating the TSTA-ELK imaging vector.
- Testing and validating activity of TSTA-ELK in cell culture.
- Creating the AdTSTA-ELK1.

- Demonstration that AdTSTA-ELK responds to MAPK signaling in live animals.
- Demonstration that MAPK levels do not differ between LAPC9 and CWR22 AD and AI xenografts but do differ between LAPC9 and CWR22 xenograft models.
- Demonstration that Iressa does not affect MAPK signaling in CWR22 tumors.

Reportable Outcomes 2002-2005:

The work funded in part by this grant has now been described in 4 publications:

1. Zhang, L., Johnson, M., Le, K., Sato, M., Ilagan, R., Iyer, M., Gambhir, S., Wu, L. and **Carey, M.** (2003). Interrogating Androgen Receptor Function in Recurrent Prostate Cancer. Cancer Research **63:** 4552-4560.
2. Sato, M., Johnson, MS, Zhang, L., Zhang, B., Le, K., Gambhir, SS., **Carey, M.,** and Wu, L. (2003). Optimization of Adenoviral Vectors to Direct Highly Amplified Prostate-Specific Expression for Imaging and Gene Therapy. Molecular Therapy **8;** 726-737.
3. Ray, S, Paulmurugan, R, Hildebrandt, I, Iyer, M, Wu L, **Carey, M,** Gambhir, SS. (2004) Novel bidirectional vector strategy for amplification of therapeutic and reporter gene expression. Hum Gene Ther. **15:**681-90.
4. Iyer, M. Salazar, F.B, Lewis, X., Zhang, JL, **Carey, M.,** Wu, L. and Gambhir SS. (2004) Non-Invasive Imaging of Enhanced Prostate-Specific Gene Expression Using a Two-Step Transcriptional Amplification Based Lentivirus Vector. Molecular Therapy **10:**545-552.
5. Sato M, Johnson M, Zhang L, Gambhir SS, **Carey M**, Wu L.(2005). Functionality of androgen receptor-based gene expression imaging in hormone refractory prostate cancer. Clin Cancer Res **11:**3743-9.
6. Iyer M, Bergara F, Lewis X, Zhang L, Wu L, **Carey M**, Gambhir SS.(2005). Noninvasive Imaging of a Transgenic Mouse Model Using a Two-Step Transcriptional Amplification Strategy. Transgenic Research **14:**47-55.
7. Ilagan R, Zhang L, Pottratz J, Le K, Salas S, Iyer M, Wu L, Gambhir SS, **Carey M** (2005). Imaging Androgen Receptor Function During Flutamide Treatment in a Prostate Cancer Xenograft. Mol Can Ther (in press).
8. Ilagan R, Pottratz J, Le K, Zhang L, Wong S, Ayala R, Iyer M, Slamon D, Wu L, Gambhir SS, and **Carey M.** Imaging MAPK Function in Xenograft Models of Prostate Cancer (submitted)

Posters: Over the past three years the work has been described in four posters at national meetings by Dr. Carey's students and in three platform presentations by Dr. Carey.

1. Abstract for 95th Annual AACR Meeting, April 2005 "Bioluminescence Imaging of AR and MAPK Activity in Androgen Independent Prostate Cancer Xenografts" Romyla Ilagan, Jill Pottratz, Kim Le, Steven Wong, Raul Ayala, Dennis Slamon and **Michael Carey.**
2. Abstract for 95th Annual AACR Meeting, March 2004. "Interrogating Androgen Receptor and MAPK Function in Androgen Independent

Prostate Cancer by Optical Imaging with Two-Step Transcription Amplification Systems." Romyla Ilagan, Liqun Joann Zhang, Kim Le and **Michael Carey.**

3. Abstract for 3rd Annual Society for Molecular Imaging, September 2004. "New Transcription-Based Vectors for Bioluminescence Imaging of AR and MAPK Activity in Recurrent Prostate Cancer." Romyla Ilagan, Liqun Joann Zhang, Jill Pottratz, Kim Le and **Michael Carey**
4. Abstract for 94th Annual AACR Meeting, July 2003. "Study of Androgen Receptor-Mediated Gene Regulation in Prostate Cancer by Molecular Imaging." Liqun Joann Zhang, Myla Ilagan, Kim H. Le, Andrea Smallwood, Sanjiv. S. Gambhir, Lily Wu, and **Michael Carey.**

Talks: Over the past three years the work has been reported in five invited talks at national meetings, two talks at Biotech/Pharmaceutical companies and one talk at an academic institution.

1. Invited Speaker, July 2005, New England Biolabs, "Mechanisms of Eukaryotic Transcriptional Activation and Application Towards Molecular Imaging"
2. Invited Speaker: Prostate Cancer: Road Map to the Future Niagara Falls, NY July 28-30, 2005. "Imaging AR and MAPK Function in Prostate Cancer."
3. Invited Speaker: 2nd Annual Pacific rim Breast and Prostate Cancer Conference, Smoke Tree Ranch, Palm Springs California, April 12-15, 2005. "Imaging MAPK and AR pathways during Prostate Cancer Progression"
4. Cedars-Sinai Hospital, March 2005. "Optical Imaging of AR and MAPK Function in Prostate Cancer"
5. Invited Speaker: Third Annual Meeting of the Society for Molecular Imaging St. Louis, MO Sept 9-12, 2004 "Two Step Transcriptional Imaging Vectors and Optical Imaging Applications"
6. Invited Speaker: Merck Pharmaceuticals, West Point, PA , July 12, 2004 "Molecular Imaging of Androgen Receptor Function in Prostate Cancer Xenografts"
7. Invited Speaker: NCI Symposium: Androgen Action in Prostate Cancer Keystone Resort, Colorado March 4-6, 2004. "Optical Imaging of AR Function in Prostate Cancer
8. Invited Speaker: Molecular Imaging of Prostate Cancer Workshop, February 1-2, 2004 Washington D.C. "Optical Imaging of AR and MAPK Genetic Pathways in Prostate Cancer Xenografts"
9. Invited Speaker: Cedars-Sinai Hospital, March 2005. "Optical Imaging of AR and MAPK Function in Prostate Cancer"

Conclusions:

The current work provides support for the concept that gene expression based optical imaging can be applied to study cancer signaling pathways in animal models.

In year 1 we described the AR-responsive AdTSTA readout system and showed that it functioned as an accurate indicator of AR activity in live animals (Zhang et al.,

2003) as compared to numerous molecular and cellular benchmarks. We also developed the single plasmid vectors for the TSTA-ELK system to measure MAPK signaling and showed that these vectors functioned in culture in response to AR and MAPK.

In year 2 we synthesized the TSTA-ELK adenovirus and began in vivo testing to determine if it can measure MAPK robustly within a xenograft tumor. We tested proof of principle by injecting a MAPK stimulant, EGF, directly into mice and measured a response. A reproducible but modest increase in optical signal was observed within the tumor in 4 hours. We also began testing the effect of a small molecule EGFR inhibitor, Iressa, in a CWR22 AI model that displayed high TSTA-ELK activity in cell culture.

In year 3 we completed two tests of the concept that TSTA-based imaging can be used to detect the effects of small molecule pharmaceuticals. In one, we showed that AdTSTA could detect the inhibitory effect of the AR antagonist flutamide in the LAPC9 xenograft model of prostate cancer. We also completed a test of Iressa on MAPK levels in LAPC9 and CWR22 xenografts. We found, unfortunately, that despite early encouraging data, there was no statistically significant inhibitory effect of Iressa on MAPK signaling or tumor growth in six separate studies employing almost 70 mice. We found that neither LAPC9 nor CWR22 AI xenografts displayed any significant difference in MAPK activity versus their AD counterparts. This challenges a widely held notion that MAPK levels are elevated in the AI versions of these models. However, the CWR22 models showed significantly higher MAPK than LAPC9.

The data and reagents generated from this project led to two published, one submitted and one in preparation papers from my lab. Reagents and data generated by this project led to 5 additional papers with my collaborators Drs. Lily Wu (UCLA) and Sam Gambhir (Stanford). The data were presented in talks at 5 national meetings and in posters at 4 meetings. The data were also presented in talks at one academic institution other than UCLA and two companies.

Our results conclusively demonstrate the ability to measure signaling environments of a tumor repetitively and non-invasively using gene expression-based imaging. The data suggest the possibility that the technology could be used clinically if we can extend the method to employ PET reporter genes. Such studies are in progress by my collaborators using reagents generated by this grant.

Personnel List: The funds were used to partially or completely to fund m the PI Micahel Carey, one postdoc (L. Joann Zhang), two graduate students (Kim Le and Myla Ilagan) and three technicians (Sussan Salas, Jill Pottratz, Kevin Terra) one of who is now in Medical School (Ms. Salas) and another in graduate school (Ms. Pottratz). The enormous cost of this project was defrayed largely by the DOD idea award but was supplemented by funds from the Jonsson Cancer Center at UCLA, developmental funds from an ICMIC grant awarded to Dr. Harvey Herschman, and a Research and Training In Pharmaceutical Science grant to Dr. Herschman and a Tumor Cell Biology Training grant awarded to Dr. Fred Fox. Details are available upon request.

References: None

Appendices:

Ilagan R, Zhang L, Pottratz J, Le K, Salas S, Iyer M, Wu L, Gambhir SS, **Carey M** (2005). Imaging Androgen Receptor Function During Flutamide Treatment in a Prostate Cancer Xenograft. Mol Can Ther (in press).

Ilagan R, Pottratz J, Le K, Zhang L, Wong S, Ayala R, Iyer M, Slamon D, Wu L, Gambhir SS, and **Carey M.** Imaging MAPK Function in Xenograft Models of Prostate Cancer (submitted)

Imaging androgen receptor function during flutamide treatment in the LAPC9 xenograft model

Romyla Ilagan,[1] Liquin Joann Zhang,[1] Jill Pottratz,[1] Kim Le,[1] Sussan Salas,[1] Meera Iyer,[3] Lily Wu,[2,3] Sanjiv S. Gambhir,[3] and Michael Carey[1]

Departments of [1]Biological Chemistry, [2]Urology, and [3]Molecular and Medical Pharmacology, School of Medicine, University of California at Los Angeles, Los Angeles, California

Abstract

The current understanding of the response of androgen receptor to pharmacologic inhibitors in prostate cancer is derived primarily from serum prostate-specific antigen (PSA) levels. In this study, we test whether a novel androgen receptor–specific molecular imaging system is able to detect the action of the antiandrogen flutamide on androgen receptor function in xenograft models of prostate cancer. Adenoviruses bearing an optical imaging cassette containing an androgen receptor–responsive two-step transcriptional amplification system were injected into androgen-dependent and hormone-refractory tumors of animals undergoing systemic time-controlled release of the antiandrogen flutamide. Imaging of tumors with a cooled charge-coupled device camera revealed that the response of AdTSTA to flutamide is more sensitive and robust than serum PSA measurements. Flutamide inhibits the androgen signaling pathway in androgen-dependent but not refractory tumors. Analysis of androgen receptor and RNA polymerase II binding to the endogenous *PSA* gene by chromatin immunoprecipitation revealed that flutamide treatment and androgen withdrawal have different molecular mechanisms. The application of imaging technology to study animal models of cancer provides mechanistic insight into antiandrogen targeting of androgen receptor during disease progression. [Mol Cancer Ther 2005;4(11):1–8]

Introduction

Prostate cancer is a disease driven by the androgen receptor (1–4). Androgen receptor is a 110-kDa steroid receptor, which is sequestered in the cytoplasm by chaperones in the absence of its ligand. In the presence of dihydrotestosterone, androgen receptor dimerizes and enters the nucleus, where it binds to androgen response elements and activates transcription of responsive genes. One of the key challenges in prostate cancer research has been determining how androgen receptor functions in recurrent or androgen-independent prostate cancer (also called hormone-refractory prostate cancer; refs. 5–11) and how pharmacologic inhibitors affect function (12). Our groups have been addressing this problem using gene expression–based bioluminescence imaging to evaluate androgen receptor function in xenograft models (13–16), which accurately recreate prostate cancer progression from an androgen-dependent to an androgen-independent phase (17).

Imaging provides a means to probe the mechanism of cancer in live animals and facilitates the evaluation of pharmacologic effects on specific signaling events. In this study, we address the mechanism of a nonsteroidal antiandrogen called flutamide by molecular imaging of androgen receptor function and compare the results with the effects of androgen deprivation by castration. Flutamide is more potent than Casodex in mice (18, 19). We chose this drug to address whether a specialized molecular imaging system could be employed to detect the inhibitory effect of an antiandrogen on androgen receptor function during prostate cancer growth.

In gene expression–based bioluminescence imaging, a promoter is placed upstream of a bioluminescence reporter gene (20–22). The reporter cassette is introduced into tumor cells in an animal and the promoter activity is imaged after injection of D-luciferin (for firefly luciferase) or coelenterazine (for *Renilla* luciferase) using a Xenogen *in vivo* imaging system (Xenogen Corp., Alameda, CA; ref. 23). *In vivo* imaging system is a cooled charge-coupled device that measures bioluminescent light. A computer interprets the light and superimposes a pseudoimage, representing the quantity of photons emitted by the tissue, over a gray-scale photograph of the animal.

A major challenge in bioluminescence imaging is that cellular promoters are typically weak, and detection of optical signals in dense tissues is hampered by light attenuation and scattering (20, 24). We developed an approach to augment cellular promoter activity and light output based on a concept termed two-step transcriptional amplification (TSTA; ref. 16). A cellular promoter expresses a potent chimeric activator, GAL4-VP16. GAL4-VP16 is a fusion of the high-affinity yeast GAL4 DNA-binding domain to the potent herpes simplex virus VP16 activation domain (25, 26). GAL4-VP16 has a unique potency and specificity not naturally found in mammalian cells. GAL4-VP16 binds a GAL4-responsive reporter gene and generates high levels of firefly luciferase. Our prostate cancer–specific

Received 6/15/05; revised 8/8/05; accepted 8/30/05.

Note: S.S. Gambhir is currently at the Molecular Imaging Program at Stanford, Stanford University School of Medicine, James H. Clark Center, E13 318 Campus Drive, Stanford, CA 94305-5472.

The costs of publication of this article were defrayed in part by the payment of page charges. This article must therefore be hereby marked advertisement in accordance with 18 U.S.C. Section 1734 solely to indicate this fact.

Requests for reprints: Romyla Ilagan, Department of Biological Chemistry, School of Medicine, University of California at Los Angeles, 10833 Le Conte Avenue, CHS 33-142, Los Angeles, CA 90095-1737. Phone: 310-794-9636; Fax: 310-206-5272. E-mail: milagan@ucla.edu

doi:10.1158/1535-7163.MCT-05-0197

version of the TSTA system employs a modified prostate-specific antigen (PSA) promoter, which responds more robustly than the native promoter to the androgen receptor (27). It also contains a more potent derivative of GAL4-VP16, where the VP16 activation domain is dimerized (GAL4-VP2; ref. 22).

We employed this optimized androgen receptor–responsive TSTA vector to generate adenovirus (AdTSTA) and lentivirus (13, 14, 28, 29), where we could sensitively measure androgen receptor signaling in xenograft tumors or native prostate tissue within live animals. An advantage of the AdTSTA approach is the ability to inject the virus into any tumor in any xenograft animal. Many of the xenografts do not exist as cell lines, placing a limitation on the development of stably transformed cells. We therefore used the adenovirus to image existing human xenografts in severe combined immunodeficient mice, and our results have addressed several questions about androgen receptor function in recurrent cancer.

Imaging of AdTSTA in LAPC9 xenografts, which express wild-type androgen receptor and PSA, revealed the loss of androgen receptor activity on androgen withdrawal by castration and the resuscitation of activity as the tumor transitioned into the recurrent state (14). Numerous biological benchmarks of androgen receptor function correlated closely with the imaging measurements. In androgen-dependent tumors, the serum PSA levels increased with tumor size, androgen receptor bound to the endogenous PSA promoter and enhancer, and RNA polymerase II was bound both at the promoter and in the act of transcribing downstream exons. Androgen withdrawal by castration led to decreased serum PSA levels, decreased androgen receptor levels, and cytoplasmic localization of androgen receptor in the xenograft tumors. Furthermore, chromatin immunoprecipitation analysis revealed a loss of androgen receptor from the PSA promoter and enhancer. Surprisingly, on castration, polymerase II remained bound at the promoter, although androgen receptor binding was substantially reduced. On transition of the tumor into the androgen-independent stage, the androgen receptor levels increased, androgen receptor relocalized to the nucleus and bound to the PSA enhancer and promoter, and polymerase II bound at both the promoter and the downstream exons. The data collectively argued that androgen receptor is fully active in androgen-independent cancer.

Much has been learned about androgen receptor response to antiandrogens in cell lines, but little is known of how antiandrogen treatment affects androgen receptor activity in androgen-dependent and recurrent tumors in animal models and how the effects compare to androgen withdrawal. In this study, we tested the effect of a nonsteroidal antiandrogen called flutamide used clinically to treat prostate cancer. Our study was designed to address three key questions: (*a*) Can androgen receptor–specific, gene expression–based imaging measure the response to the antiandrogen flutamide in a living subject? (*b*) Is imaging more sensitive than conventional benchmarks, such as serum PSA levels or tumor size? and (*c*) Does inhibition of the androgen signaling pathway by flutamide employ a similar mechanism as androgen deprivation in the context of the tumor?

We found that AdTSTA was more sensitive than serum PSA in measuring the inhibitory effect of flutamide. The imaging measurements allowed us to identify time points at which to analyze changes in androgen receptor within the tumor environment that accompany the onset of the therapeutic effect. These alterations suggest fundamental differences between androgen withdrawal and antiandrogen treatment, which may be related to the mechanism of hormone resistance.

Materials and Methods

Animal Charge-Coupled Device Experiments

The imaging was done essentially as we described previously (13). Animal care and euthanasia were done with the approval of the University of California at Los Angeles Animal Research Committee. The mice were first anesthetized with ketamine-xylazine mix (4:1). Imaging was done using a Xenogen *in vivo* imaging system 100 cooled charge-coupled device camera. The mice were injected with 200 μL of 15 mg/mL D-luciferin i.p. 15 minutes before imaging, after which they were placed in a light-tight chamber. A gray-scale reference image was obtained followed by the acquisition of a bioluminescent image. The acquisition time ranged from 1 to 2 minutes. The images shown are pseudoimages of the emitted light in photons/s/cm^2/steradian superimposed over the gray-scale photographs of the animal. We used LAPC9 animals bearing tumors of 0.4 cm in diameter to study the flutamide response as larger tumors were relatively unresponsive. Briefly, on day 1, 10^7 plaque-forming units of AdTSTA were injected in two locations. Imaging generally commenced 3 days later. On day 3, flutamide (25 mg/60-day release) or placebo pellets (Innovative Research) were implanted s.c. on the dorsal side of the mouse. Time courses were done where mice were imaged every 3 to 4 days. Because adenoviral injection delivers slightly different amounts of vector to the tumors due to viral leakage, we obtained a baseline image 3 days after viral injection and measured the percent change in signal over time. The data were analyzed statistically using Student's *t* test as described previously (14).

Immunoblots

Whole tumors were harvested from mice via surgical removal at the imaging end points and immediately frozen in liquid N_2. Frozen tumors were homogenized using a mortar and pestle in the presence of liquid N_2. Samples were then resuspended in 400 to 600 μL radioimmunoprecipitation assay buffer (10 mmo/L Tris-HCl, 1% NP40, 1% sodium deoxycholate, 150 mmo/L NaCl, 1 mmo/L EDTA, 0.2% SDS, 1 mmo/L phenylmethylsulfonyl fluoride, 1 μg/mL leupeptin and pepstatin, 1 mmo/L Na_3VO_4, 1 mmo/L NaF). Lysates were passed through 25-gauge needles to shear genomic DNA followed by

centrifugation at 14,000 × *g* at 4°C for 20 minutes. Samples were assayed for total protein concentration Q6 using the Pierce BCA Protein Assay kit and further normalized using γ-tubulin or cytokeratin-8 antibodies for loading controls. Extracts were fractionated on 4% to 15% Tris-HCl Ready Gels and immunoblotted. Antibodies against androgen receptor M-441 (sc-7305), γ-tubulin (D-10; sc-17788), and cytokeratin-8 (sc-802) were obtained Q7 from Santa Cruz Biotechnology. Antibodies to transcription factor IIB were generated in our laboratory.

Chromatin Immunoprecipitation

Chromatin immunoprecipitation was done on formaldehyde cross-linked tumor samples essentially as described using antibodies to androgen receptor and polymerase II (14).

Results

Imaging Provides a Sensitive Indicator of Androgen Receptor Inhibition

Figure 1A illustrates the androgen receptor–responsive, gene expression–based imaging cassette inserted within AdTSTA and used in the experiments described below (14). The system sensitively measures androgen receptor activity in prostate tissues by expressing firefly luciferase, which is detected using a Xenogen *in vivo* imaging system. Our previous studies have shown that the amount of firefly luciferase activity is proportional to the activity of androgen receptor both *in vitro* and in animals (13, 14). Further, the AdTSTA approach was highly successful in quantifying the loss of tumor androgen receptor function by castration and the resuscitation of activity as the tumor transitioned to a recurrent phase. Based on these results, we surmised that the system would be able to detect the effect of small-molecule inhibitors directed at androgen receptor.

One of the strengths of the AdTSTA imaging system is the ability to noninvasively and repetitively monitor individual animals to compare the signaling pathway with clinical measurements of tumor function. Figure 1 shows the results of a typical experiment, where two intact male severe combined immunodeficient mice bearing LAPC9 tumors were injected with AdTSTA (day 1) after the tumors had reached ~0.4 cm average diameter by caliper measurement. After taking a baseline charge-coupled device measurement on day 3 following injection of AdTSTA, the two mice were implanted with either a flutamide time-release pellet or a placebo pellet. We then

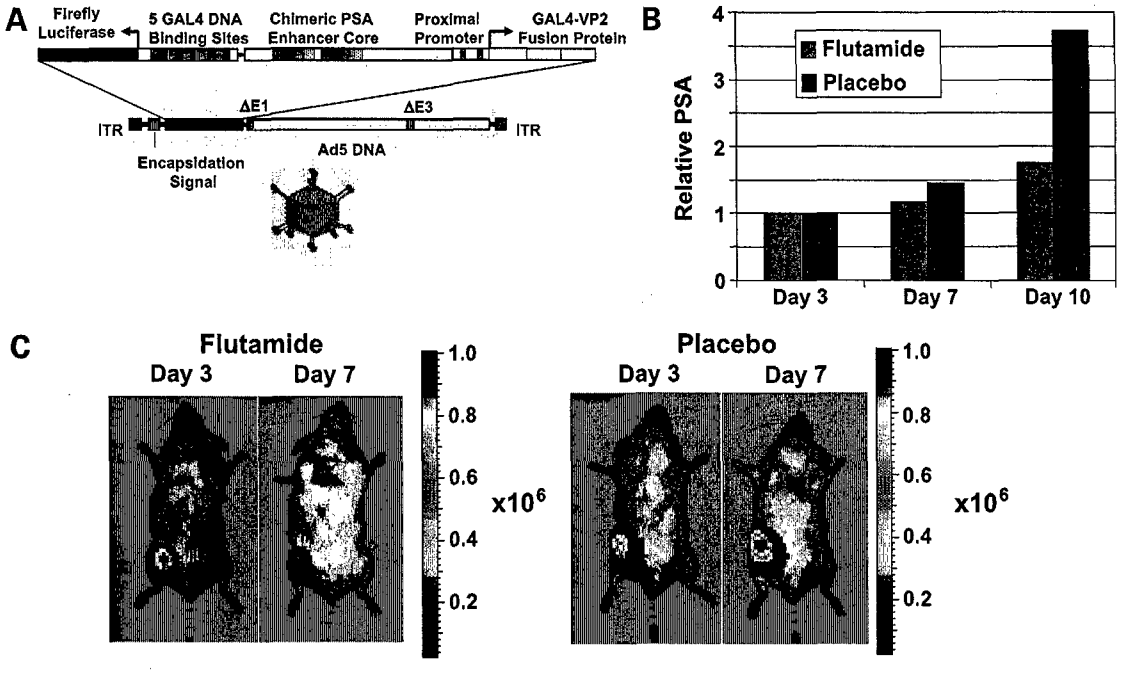

Figure 1. AdTSTA detects response of androgen-dependent tumors to flutamide. **A,** AdTSTA cassette. AdTSTA contains two copies of the PSA enhancer placed upstream of the natural promoter (13, 27). Immediately downstream of the start site is a gene encoding GAL4-VP2, a fusion of amino acids 1 to 147 of GAL4, containing the GAL4 DNA-binding domain, fused to two copies of the herpes simplex virus VP16 activation domain (amino acids 413-454; ref. 26). A GAL4-responsive reporter gene is positioned upstream of the PSA enhancers but in the opposite direction. The reporter contains five GAL4 sites upstream of the adenovirus E4 promoter driving firefly luciferase. **B,** serum PSA levels. Serum was taken from the mice by orbital bleed and subjected to serum PSA measurements using the American Qualex PSA ELISA kit (KD4310). The two levels were normalized to 1, and the fold change over time was monitored on days 7 and 10 postinjection. *Columns,* average of triplicate serum PSA measurements ($n = 6$; $P = 0.049$). **C,** inhibition by flutamide in typical animals. LAPC9 tumors were grown to 0.4 cm in severe combined immunodeficient mice and injected on day 0 with AdTSTA. On day 3 postinjection of AdTSTA, a baseline image was taken using a Xenogen *in vivo* imaging system charge-coupled device camera and the mice were implanted with placebo or flutamide slow-release pellets (25 mg/60-day release). The mice were imaged on day 7 to monitor the short-term effects of flutamide on the androgen receptor pathway. Typical images are shown. The firefly luciferase activity is measured in light units of photons/s/cm^2/steradian. Q8

monitored the change in signal over time versus the baseline measurement. In parallel, we measured the PSA levels of the animals to compare with the imaging measurements. Figure 1B shows that significant PSA differences between placebo-treated and flutamide-treated animals are only observed on day 10. However, the charge-coupled device images in Fig. 1C shows that on day 7 postinjection, when PSA levels have not changed significantly, the imaging detects an increase in androgen receptor signaling in the placebo-treated animal and a decrease in the flutamide-treated animal. We conclude that the TSTA system can detect the antiandrogenic effects of flutamide paralleling the clinical effects of the antiandrogen in man.

Pathway Inhibition Versus Tumor Growth and PSA

A key issue in understanding the action of pharmacologic inhibitors is whether the inhibitor reaches its site of action in living subjects and whether inhibition of the pathway truly inhibits tumor growth to the same extent. The experiment in Fig. 2 addresses this issue by comparing the flutamide responses of the AdTSTA imaging system, serum PSA levels, and tumor size over time. The three graphs illustrate the changes in average charge-coupled device signals (Fig. 2A), tumor sizes (Fig. 2B), and serum PSA levels (Fig. 2C) for the flutamide (n = 9) and placebo (n = 6) cohorts from 3 to 18 days after injection of the AdTSTA imaging vector. The imaging signal increases on day 7, 4 days after the placebo and flutamide pellets were implanted, and then begins to drop gradually over time. The increase in signal is expected as the virus begins to respond to the cellular environment and generates increased levels of luciferase. After steady-state levels are reached, the signals begin to diminish in LAPC9 androgen-dependent tumors. AdTSTA, unlike the tumor cells, does not replicate and the optical signal diminishes gradually as the tumor burden increases due to increased light absorption by the tissue. Despite this caveat, there is a significant and consistent difference averaging ~250% in the charge-coupled device signal between the placebo and the flutamide cohorts from day 7 (P = 0.03) to day 18 (P = 0.004).

The differences in PSA levels were noticeable on day 10, but the P was not significant (P = 0.3). As the tumors reached their maximal sizes on day 18 (Fig. 2B), the difference between treated and untreated cohorts became apparent but not statistically significant. This was not as accurate as the imaging values (P = 0.004). We conclude that imaging detects a significant reduction of androgen receptor signaling at time points where PSA levels are similar.

Androgen Receptor Levels and Chromatin Immunoprecipitation in Flutamide-Treated Tumors

To further understand the molecular consequences of flutamide action on androgen receptor, we employed the imaging analysis to identify time points when the effect of flutamide was evident (4 days after initiating treatment). At this stage, tumors were harvested and subjected to immunoblot and chromatin immunoprecipitation analyses to determine the levels of androgen receptor and its ability to bind the PSA enhancer.

Comparison of androgen receptor levels in tumors from animals castrated 4 days before harvest revealed that androgen receptor levels decrease significantly relative to several other gel loading controls, such as γ-tubulin and transcription factor IIB (Fig. 3A). We reported previously that this decrease was associated with reduced serum PSA levels and a reduced AdTSTA imaging signal. Additionally, chromatin immunoprecipitation analysis revealed a significant decrease in binding of androgen receptor to the PSA enhancer and promoter in castrated state and a increase in the androgen-independent state (14).

In contrast to the results in castrated animals, we observed a consistent 2-fold increase in androgen receptor levels 4 days after treatment in the flutamide-treated versus

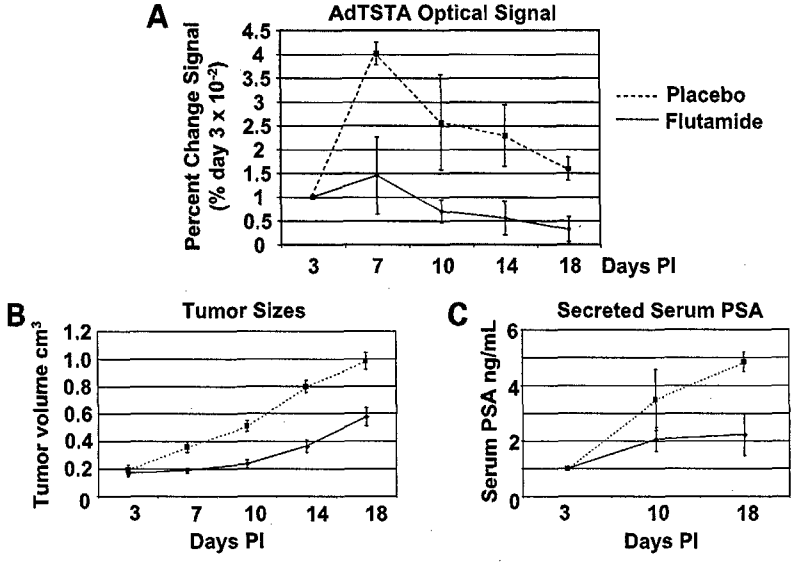

Figure 2. Comparison of imaging signals, PSA levels, and tumor volumes for cohorts. **A,** imaging of LAPC animals. Cohorts of nine flutamide-treated and six placebo-treated animals were subjected to imaging. The maximal imaging signals for the placebo and flutamide cohorts were averaged and plotted as the percent change versus the baseline image taken on day 3 postinjection (*PI*) of AdTSTA. **B,** tumor volumes were estimated based on the average diameter using calipers. Measurements were taken at the indicated time points. The percent changes versus the values measured on day 3 were measured and averaged. *Points,* mean; *bars,* SD. Student's t test was used to determine significance. **C,** PSA levels were measured by serum ELISA and measured in parallel to the imaging. Blood samples were taken by retro-orbital sinus bleed from alternating eyes according to the University of California at Los Angeles Animal Research Committee regulations. Values were averaged on day 3, and placebo- and flutamide-treated cohorts were separated and measured on days 10 and 18.

placebo-treated animals as shown for two representative individuals each (Fig. 3B). The data suggest that flutamide stabilizes androgen receptor in the tumor, much like the effect of dihydrotestosterone (30, 31).

A key question was whether transcription complexes were forming on the *PSA* gene. Flutamide and a related inhibitor Casodex (bicalutamide), not used in this study, have been widely reported as facilitating the nuclear localization of androgen receptor, and previous reports have suggested that bicalutamide promotes binding of androgen receptor to the PSA regulatory region in LNCaP cell lines (32–34). Additionally, we reported previously that transcription factors, including polymerase II, remained bound to the promoter of the *PSA* gene under conditions where castration had led to decreased levels and binding of androgen receptor in LAPC9 tumors (14). We therefore probed the PSA enhancer in the LAPC9 tumors by chromatin immunoprecipitation to determine if the enhanced levels of androgen receptor reflect functional binding even while the *PSA* gene is relatively inactive. Figure 4B shows that androgen receptor is indeed bound to the PSA enhancer in the presence and absence of flutamide (compare *lanes 1* and 2). Although androgen receptor is bound in androgen-independent tumors, it is bound less well consistent with the decreased androgen receptor levels typically found in our xenograft model.

Although androgen receptor is bound to the promoter, the imaging and PSA data suggest that the gene is largely inactive. To confirm that transcription was indeed inactivated, we probed the promoter for the presence of RNA polymerase II (Fig. 4C). Although polymerase II is bound to the PSA promoter in androgen-dependent, androgen-independent, and castrated tumors, it nearly disappears from the promoter in the presence of flutamide despite the presence of androgen receptor at the enhancer. The data illustrate that in the context of the tumor the effects of androgen withdrawal by castration and the antiandrogenic effects of flutamide are fundamentally different.

Flutamide Insensitivity in Androgen-Independent Cancer

The inability of the antiandrogens flutamide and Casodex to inhibit androgen receptor in androgen-independent cancer is one of the reasons men eventually die from metastatic disease (35). Although these drugs elicit transient effects in patients, the androgen insensitivity of the tumor prevents the drugs from functioning. Indeed, in some individuals, flutamide and Casodex begin to act as agonists (36–38).

Figure 5 compares the effect of placebo and flutamide treatment on androgen receptor activity in androgen-dependent and androgen-independent LAPC9 tumors. Whereas the androgen-dependent tumors are grown in intact male mice, the androgen-independent tumors are stably propagated in castrated male severe combined immunodeficient mice. Figure 5A shows that in typical animals, by day 18, the imaging signal in androgen-dependent tumors has decreased below the baseline

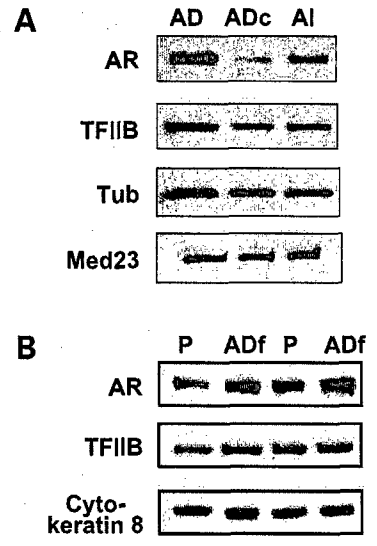

Figure 3. Androgen receptor levels in treated tumors. Whole-cell tumor extracts were prepared by freezing tumors in liquid N_2 followed by crushing with a mortar and pestle. The crushed tissue was resuspended in radioimmunoprecipitation assay buffer, heated, and fractionated on SDS polyacrylamide gels. The extracts were blotted onto nitrocellulose and normalized to γ-tubulin (*Tub*) or cytokeratin-8. **A**, comparison of androgen-dependent, castrated, and androgen-independent tumors. *AD*, extract from tumors grown in intact male mice; *Adc*, samples from androgen-dependent tumors after castration (castration was done 4 d before harvest of the tumor); *AI*, tumors grown in castrate mice. **B**, effects of flutamide. *P* and *Adf*, tumors treated with placebo or flutamide, respectively, for 4 d. The blots were developed by chemiluminescence. Representative data are shown. Fold differences were determined using Molecular Dynamics laser densitometer using ImageQuant 5.2 software. Q9

observed on day 3 (compare the animals in Fig. 5A, *top*). In contrast, we observe no inhibition of androgen receptor function in androgen-independent tumors over the same period.

These observations are reflected in the graph, which plots the change in signal from days 3 to 18 in placebo- and flutamide-treated cohorts (Fig. 5B). In placebo-treated animals, the optical signals were higher relative to flutamide-treated tumors by day 18 consistent with the previous experiment ($P = 0.045$; see Fig. 2). In contrast, the signals in the flutamide-treated androgen-independent animals were similar to the placebo cohort.

Discussion

The use of bioluminescence imaging in combination with molecular analysis is an emerging paradigm for tumor studies in preclinical models of cancer. An important application of imaging is to determine whether a drug is reaching its intended target within a living subject and to determine whether the efficacy of target inhibition correlates with the therapeutic effect. This latter issue represents a key challenge in the pharmaceutical industry, as it is difficult to ascertain whether the failure of a drug is due to its inability to reach the target or whether the target is not influencing cancer

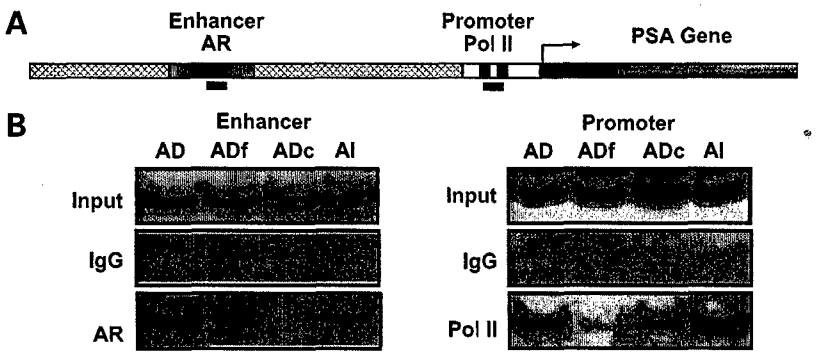

Figure 4. Chromatin immunoprecipitation of androgen receptor and polymerase II (*pol II*) in flutamide-treated tumors. **A,** schematic of the PSA regulatory region and location of primer sets surrounding androgen receptor sites in the enhancer and promoter. Sequence details on the primers can be found in ref. 14. **B,** binding of androgen receptor to the enhancer. Androgen receptor or IgG antibodies were used to immunoprecipitate sheared chromatin from formaldehyde cross-linked tumors isolated from mice bearing LAPC9 androgen-dependent, flutamide-treated androgen-dependent tumors, tumors from mice castrated 10 d before harvest, and tumors stably grown in castrate animals. The DNA in the precipitates was amplified using the primers to the PSA enhancer, which amplifies the region containing multiple androgen receptor–binding sites. Input samples represent 2% of the starting sample before chromatin immunoprecipitation. **C,** polymerase II binding to the proximal promoter was measured by chromatin immunoprecipitation using a polymerase II CTD antibody (Covance). IgG is a mock immunoprecipitation to assess background levels of precipitation. Q10

growth. A second application of imaging is to identify periods when a drug is displaying maximal efficacy to perform invasive analyses to understand the mechanism of inhibition.

We employed the antiandrogen flutamide to test the ability of our TSTA molecular imaging system to measure the effect of a known small-molecule pharmaceutical on a specific signaling pathway in a live animal and to contrast the effects with our previous study on another standard treatment, androgen deprivation. We used adenovirus to deliver the TSTA imaging system because the xenografts used here do not grow as lines in cell culture and hence cannot be stably transformed with an imaging vector.

Our study led to the following conclusions: Flutamide significantly inhibits androgen receptor function in androgen-dependent prostate cancer xenografts, although the magnitude of the inhibition seems less than that observed by androgen withdrawal (~3-fold for flutamide and 10-fold for androgen withdrawal) reported in our previous

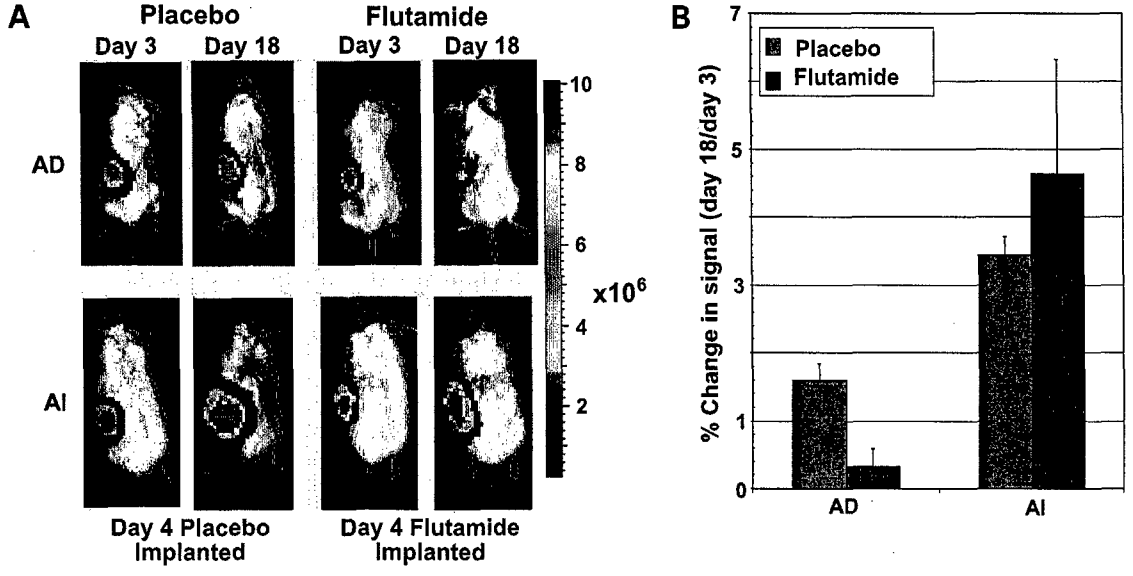

Figure 5. LAPC9 androgen-independent tumors are resistant to flutamide. AdTSTA were injected i.t. into intact or castrated male mice bearing LAPC9 xenografts. **A,** typical effects. On day 3, a baseline image was acquired and flutamide or placebo pellets were implanted. The effect of treatment at day 18 is shown. We have not detected any flutamide effect in the LAPC9 androgen-independent tumor model. **B,** cohorts of androgen-dependent (n = 7) and androgen-independent (n = 6) animals were studied. *Columns,* percent change in signal versus day 3 in placebo- and flutamide-treated animals bearing androgen-dependent and androgen-independent tumors.

study. The imaging signal and trends accurately recapitulate the effect of the flutamide on PSA levels, a clinical benchmark of prostate cancer. Yet, imaging with AdTSTA was more sensitive than serum PSA levels and reliably identified flutamide-mediated inhibition at earlier time points. Despite our previous observation that androgen receptor is fully active in androgen-independent cancer (14), androgen receptor signaling is highly resistant to flutamide inhibition.

With imaging, we were able to identify time points when the effect of flutamide was immediately evident and then harvest tumors to evaluate the molecular effects using immunoblotting and chromatin immunoprecipitation. From these analyses, we made the following observations. In contrast to the effects of androgen withdrawal by castration, flutamide did not inhibit androgen receptor binding to the PSA regulatory region but did inhibit polymerase II binding to the promoter. This effect occurred despite the observation that levels of androgen receptor and several of its coactivators are elevated in flutamide-treated tumors. Therefore, we conclude that antiandrogens and androgen withdrawal have distinct mechanisms of inhibition within the context of a tumor.

One of the key differences between the effects of androgen withdrawal and flutamide is the level of androgen receptor. In castrated animals, the tumor levels of androgen receptor decrease at the earliest time point, where the imaging revealed the inhibition. In contrast, flutamide increases the levels of androgen receptor at points where the inhibition is initially observed. The data are reminiscent of the stabilizing effect of dihydrotestosterone on androgen receptor (30, 31).

Our previous data along with cell culture studies show that castration or androgen deprivation causes the remaining androgen receptor to localize largely in the cytoplasm. Flutamide and Casodex, however, promote nuclear localization (39–41), which may in turn enhance androgen receptor stability and DNA binding. Consistent with this notion was our observation that androgen receptor binding to the PSA enhancer clearly decreases in tumors of castrate mice but remains bound in flutamide. Androgen receptor binding also occurs in LNCaP cells in the presence of another antiandrogen bicalutamide (42).

Polymerase II seems to bind the PSA promoter in castrate animals, although it is generally not found within the coding region. In contrast, we find little polymerase II bound to the promoter in the presence of flutamide. This observation in the tumor is consistent with cell culture studies showing that Casodex may actively repress the *PSA* gene by permitting androgen receptor to interact with corepressors (32, 43, 44). In addition, flutamide decreases the association of androgen receptor with various coactivators including TIF2, which in turn affects androgen receptor–mediated transcriptional activity (43, 45). Therefore, it is more likely that flutamide inhibits androgen receptor–mediated transcription through rearranging the cofactor environment on a promoter than affecting nuclear localization and DNA binding.

References

1. Feldman BJ, Feldman D. The development of androgen-independent prostate cancer. Nat Rev Cancer 2001;1:34–45.
2. Gelmann EP. Molecular biology of the androgen receptor. J Clin Oncol 2002;20:3001–15.
3. Cronauer MV, Schulz WA, Burchardt T, et al. The androgen receptor in hormone-refractory prostate cancer: relevance of different mechanisms of androgen receptor signaling [review]. Int J Oncol 2003;23:1095–102.
4. Schulz WA, Burchardt M, Cronauer MV. Molecular biology of prostate cancer. Mol Hum Reprod 2003;9:437–48.
5. Chen CD, Welsbie DS, Tran C, et al. Molecular determinants of resistance to antiandrogen therapy. Nat Med 2004;10:33–9.
6. Mellinghoff IK, Tran C, Sawyers CL. Growth inhibitory effects of the dual ErbB1/ErbB2 tyrosine kinase inhibitor PKI-166 on human prostate cancer xenografts. Cancer Res 2002;62:5254–9.
7. Mellinghoff IK, Vivanco I, Kwon A, Tran C, Wongvipat J, Sawyers CL. HER2/*neu* kinase-dependent modulation of androgen receptor function through effects on DNA binding and stability. Cancer Cell 2004;6:517–27.
8. Mohler JL, Gregory CW, Ford OH III, et al. The androgen axis in recurrent prostate cancer. Clin Cancer Res 2004;10:440–8.
9. Weber MJ, Gioeli D. Ras signaling in prostate cancer progression. J Cell Biochem 2004;91:13–25.
10. Culig Z. Androgen receptor cross-talk with cell signalling pathways. Growth Factors 2004;22:179–84.
11. Edwards J, Bartlett JM. The androgen receptor and signal-transduction pathways in hormone-refractory prostate cancer. Part 2. Androgen-receptor cofactors and bypass pathways. BJU Int 2005;95:1327–35.
12. Asatiani E, Gelmann EP. Targeted therapies for prostate cancer. Expert Opin Ther Targets 2005;9:283–98.
13. Zhang L, Adams JY, Billick E, et al. Molecular engineering of a two-step transcription amplification (TSTA) system for transgene delivery in prostate cancer. Mol Ther 2002;5:223–32.
14. Zhang L, Johnson M, Le KH, et al. Interrogating androgen receptor function in recurrent prostate cancer. Cancer Res 2003;63:4552–60.
15. Sato M, Johnson M, Zhang L, et al. Optimization of adenoviral vectors to direct highly amplified prostate-specific expression for imaging and gene therapy. Mol Ther 2003;8:726–37.
16. Iyer M, Wu L, Carey M, Wang Y, Smallwood A, Gambhir SS. Two-step transcriptional amplification as a method for imaging reporter gene expression using weak promoters. Proc Natl Acad Sci U S A 2001;98:14595–600.
17. Craft N, Shostak Y, Carey M, Sawyers CL. A mechanism for hormone-independent prostate cancer through modulation of androgen receptor signaling by the HER-2/neu tyrosine kinase. Nat Med 1999;5:280–5.
18. Singh SM, Gauthier S, Labrie F. Androgen receptor antagonists (antiandrogens): structure-activity relationships. Curr Med Chem 2000;7:211–47.
19. Luo S, Martel C, Chen C, et al. Daily dosing with flutamide or Casodex exerts maximal antiandrogenic activity. Urology 1997;50:913–9.
20. Massoud TF, Gambhir SS. Molecular imaging in living subjects: seeing fundamental biological processes in a new light. Genes Dev 2003;17:545–80.
21. Choy G, Choyke P, Libutti SK. Current advances in molecular imaging: noninvasive *in vivo* bioluminescent and fluorescent optical imaging in cancer research. Mol Imaging 2003;2:303–12.
22. Ray S, Paulmurugan R, Hildebrandt I, et al. Novel bidirectional vector strategy for amplification of therapeutic and reporter gene expression. Hum Gene Ther 2004;15:681–90.
23. Bhaumik S, Lewis XZ, Gambhir SS. Optical imaging of *Renilla* luciferase, synthetic *Renilla* luciferase, and firefly luciferase reporter gene expression in living mice. J Biomed Opt 2004;9:578–86.
24. Herschman HR. Molecular imaging: looking at problems, seeing solutions. Science 2003;302:605–8.
25. Sadowski I, Ma J, Triezenberg S, Ptashne M. GAL4-VP16 is an unusually potent transcriptional activator. Nature 1988;335:563–4.
26. Emami KH, Carey M. A synergistic increase in potency of a multimerized VP16 transcriptional activation domain. EMBO J 1992;11:5005–12.

27. Wu L, Matherly J, Smallwood A, et al. Chimeric PSA enhancers exhibit augmented activity in prostate cancer gene therapy vectors. Gene Ther 2001;8:1416 – 26.

28. Iyer M, Salazar FB, Lewis X, et al. Noninvasive imaging of enhanced prostate-specific gene expression using a two-step transcriptional amplification-based lentivirus vector. Mol Ther 2004;10:545 – 52.

29. Sato M, Johnson M, Zhang L, Gambhir SS, Carey M, Wu L. Functionality of androgen receptor-based gene expression imaging in hormone refractory prostate cancer. Clin Cancer Res 2005;11:3743 – 9.

30. Zhou ZX, Lane MV, Kemppainen JA, French FS, Wilson EM. Specificity of ligand-dependent androgen receptor stabilization: receptor domain interactions influence ligand dissociation and receptor stability. Mol Endocrinol 1995;9:208 – 18.

31. Kemppainen JA, Wilson EM. Agonist and antagonist activities of hydroxyflutamide and Casodex relate to androgen receptor stabilization. Urology 1996;48:157 – 63.

32. Shang Y, Myers M, Brown M. Formation of the androgen receptor transcription complex. Mol Cell 2002;9:601 – 10.

33. Comuzzi B, Lambrinidis L, Rogatsch H, et al. The transcriptional co-activator cAMP response element-binding protein-binding protein is expressed in prostate cancer and enhances androgen- and anti-androgen-induced androgen receptor function. Am J Pathol 2003;162:233 – 41.

34. Kim J, Jia L, Tilley WD, Coetzee GA. Dynamic methylation of histone H3 at lysine 4 in transcriptional regulation by the androgen receptor. Nucleic Acids Res 2003;31:6741 – 7.

35. Nelson WG, De Marzo AM, Isaacs WB. Prostate cancer. N Engl J Med 2003;349:366 – 81.

36. Veldscholte J, Ris-Stalpers C, Kuiper GG, et al. A mutation in the ligand binding domain of the androgen receptor of human LNCaP cells affects steroid binding characteristics and response to anti-androgens. Biochem Biophys Res Commun 1990;173:534 – 40.

37. Matias PM, Carrondo MA, Coelho R, et al. Structural basis for the glucocorticoid response in a mutant human androgen receptor (AR(ccr)) derived from an androgen-independent prostate cancer. J Med Chem 2002;45:1439 – 46.

38. Hara T, Miyazaki J, Araki H, et al. Novel mutations of androgen receptor: a possible mechanism of bicalutamide withdrawal syndrome. Cancer Res 2003;63:149 – 53.

39. Karvonen U, Janne OA, Palvimo JJ. Pure antiandrogens disrupt the recruitment of coactivator GRIP1 to colocalize with androgen receptor in nuclei. FEBS Lett 2002;523:43 – 7.

40. Tomura A, Goto K, Morinaga H, et al. The subnuclear three-dimensional image analysis of androgen receptor fused to green fluorescence protein. J Biol Chem 2001;276:28395 – 401.

41. Tyagi RK, Lavrovsky Y, Ahn SC, Song CS, Chatterjee B, Roy AK. Dynamics of intracellular movement and nucleocytoplasmic recycling of the ligand-activated androgen receptor in living cells. Mol Endocrinol 2000;14:1162 – 74.

42. Masiello D, Cheng S, Bubley GJ, Lu ML, Balk SP. Bicalutamide functions as an androgen receptor antagonist by assembly of a transcriptionally inactive receptor. J Biol Chem 2002;277: 26321 – 6.

43. Berrevoets CA, Umar A, Trapman J, Brinkmann AO. Differential modulation of androgen receptor transcriptional activity by the nuclear receptor co-repressor (N-CoR). Biochem J 2004;379:731 – 8.

44. Kang Z, Janne OA, Palvimo JJ. Coregulator recruitment and histone modifications in transcriptional regulation by the androgen receptor. Mol Endocrinol 2004;18:2633 – 48.

45. Matsuda T, Junicho A, Yamamoto T, et al. Cross-talk between signal transducer and activator of transcription 3 and androgen receptor signaling in prostate carcinoma cells. Biochem Biophys Res Commun 2001;283: 179 – 87.

Imaging MAPK Function in Xenograft Models of Prostate Cancer

By

Romyla Ilagan[1], Jill Pottratz[1], Kim Le[1], Liqun Zhang[1], Steven G. Wong[4], Raul Ayala[4], Meera Iyer[3], Lily Wu[2,3], Sanjiv S Gambhir[3,5], and Michael Carey[1]

[1]Departments of Biological Chemistry, [2]Urology, [3]Molecular and Medical Pharmacology and Medicine, [4]Medicine-Hematology and Oncology

David Geffen School of Medicine at the University of California,

Los Angeles, CA 90095

Current Address:

[5]Stanford University School of Medicine

Molecular Imaging Program at Stanford (MIPS)

Stanford University

James H. Clark Center, E13

318 Campus Drive

Stanford, CA 94305-5472

Running Title: Imaging MAPK Function in Prostate Cancer

Key words: androgen receptor, MAPK, ERK1/2, bioluminescence imaging, prostate cancer, and xenografts.

Abbreviations: AD, androgen dependent prostate cancer; AdTSTA, adenoviral vector containing two-step transcriptional amplification cassette with GAL4-VP16; AdTSTA-ELK, adenoviral vector containing two-step transcriptional amplification cassette with GAL4-ELK1; AI, androgen independent prostate cancer; ARE, androgen response elements; AR, androgen receptor; CCD, charged coupled device; CWR22, Case Western Reserve University prostate cancer xenograft model; DHT, dihydrotestosterone; EGF, epidermal growth factor; ELK1, Ets-like transcription factor; ERK1/2, extracellular signal regulated kinase 1 or 2; FLuc, firefly luciferase; GAL4-ELK1, fusion protein consisting of the GAL4 DNA binding domain fused to activation domain of ELK1 protein; GAL4-VP16, fusion protein consisting of the GAL4 DNA binding domain fused to the activation domain of the Herpes Simplex VP16 transcription factor; IVIS, *in vivo* imaging system; LNCaP, lymph node metastatic PCa cell line; LAPC9, Los Angeles Prostate Cancer 9 xenograft; MAPK, mitogen

activated protein kinase; PCa, prostate cancer or carcinoma of the prostate; PSA, prostate specific antigen; RLuc, renilla luciferase; RTK, receptor tyrosine kinase; SCID, severe combined immunodeficient syndrome; TSTA, two-step transcriptional amplification system.

ABSTRACT

Elevated activities of ERK1/2, members of the mitogen activated protein kinase (MAPK) family, are a hallmark of malignancy. Here we describe a gene expression-based imaging system that detects and quantifies ERK1/2 activity in prostate cancer tumors implanted into SCID mice. The imaging technology employs a modified version of two-step transcriptional amplification (TSTA). The tissue specificity of gene expression is imparted by an enhanced version of the PSA regulatory region that expresses GAL4-ELK1. GAL4-ELK1 confers MAPK specificity by activating a firefly luciferase reporter gene only when the ELK1 activation domain is phosphorylated by ERK1/2. Firefly luciferase activity in live animals was detected using the Xenogen *In vivo* Imaging System. We validated the TSTA-ELK1 system by analyzing its response to EGF treatment in transfected tissue culture cells and in adenovirus(AdTSTA-ELK1)-injected PCa xenograft tumors. We then employed the system to determine whether elevated ERK1/2 is associated with the progression of PCa from an androgen-dependent to an independent state in two well-characterized xenograft models, CWR22 and LAPC9. Although no significant differences were detected between AD and AI xenografts, the CWR22 models display >100-fold higher levels of AdTSTA-ELK1 activity versus LAPC9. We discuss the implications of this finding on the role of MAPK in PCa. The development of binary gene expression based imaging systems that allow tissue specific measurement of kinase activities will facilitate the analysis of signaling pathways during cancer progression and the response of tumors to specific pharmaceutical treatments.

INTRODUCTION

Elevated mitogen activated protein kinase (MAPK) activity is a hallmark of many malignancies (1, 2). Among the three branches of the MAPK pathways the extracellular response kinases (ERK1/2) stand out because cytokine receptors such as Epidermal Growth Factor (EGF) Receptor (EGFR) stimulate growth by causing phosphorylation of ERK1/2. Binding of EGF to EGFR induces the RAS signaling cascade that ultimately leads to phosphorylation of ERK by MEK. ERK phosphorylates the transcription factor ELK1 and other targets to stimulate cell proliferation (3). The MAPK pathway has been hypothesized to play a significant role in prostate cancer (PCa) by intersecting with the androgen receptor (AR).

Prostate cancer is initially dependent on AR function (4). AR is a 110-KDa steroid receptor, which is sequestered in the cytoplasm in the absence of its ligand. In the presence of dihydrotestosterone, AR dimerizes and enters the nucleus, binds to androgen response elements (AREs) and activates transcription of responsive genes (5). In the recurrent or androgen independent (AI) phase of cancer AR activity is resuscitated. One of the key challenges has been determining how AR functions in AI PCa (6, 7).

The AI phase of PCa has been associated with AR gene amplification, overexpression of AR and hyperactivation of various growth factor pathways (8). It has been reported that increased MAPK phosphorylation occurs during PCa progression in man. Phospho-MAPK1/2 levels in advanced and metastatic prostate tumors correlate with increasing Gleason score (9). Numerous receptor tyrosine kinase (RTK) pathways increase AR-mediated transactivation in cell culture (10). The RTK HER2/neu is overexpressed in a subset of breast cancers and activates estrogen receptor in a ligand-independent manner (11). HER2 is also overexpressed in a subline of the LAPC4 PCa xenograft and forced expression of HER2/neu in cell lines facilitates the transition of AD to AI growth in SCID mice (12). Use of the dual HER1/HER2 tyrosine kinase inhibitor PKI-166 inhibits the growth of at least one human prostate xenograft (13). The mechanism by which AR is activated is unknown. However, EGF increases the sensitivity of AR to ligand in the recurrent PCa cell line CWR-R1 through a mechanism whereby the coactivator TIF2/GRIP1 is phosphorylated (14). AR also appears to directly interact with the SH3 domain of Src thereby activating the ERK signal transduction cascade, which implies that MAPK activation accompanies AR function (15-17).

To further understand the role of MAPK in PCa our groups have been attempting to decipher the activity of the AR and MAPK pathways in live animals using gene expression-based bioluminescence imaging. Our studies employ xenograft models that recreate PCa progression from an AD to an AI phase (18, 19). Imaging of the xenografts allows us to pose questions about the mechanism of cancer in live animals and facilitates the evaluation of pharmacologic effects.

In gene-expression-based bioluminescence imaging, a promoter is placed upstream of a bioluminescence reporter gene (20-23). The reporter cassette is introduced into tumor cells in an animal and the promoter activity is imaged using a Xenogen *In vivo* imaging system (IVIS) after injection of the animals with D-Luciferin (for FLuc) or coelenterazine (for RLuc) (24). IVIS is a cooled charge coupled device (CCD) that measures bioluminescent light. A computer interprets the light and superimposes a pseudoimage, representing the quantity of photons emitted by the tissue, over a gray scale photograph of the animal.

A major challenge in bioluminescence imaging is that cellular promoters are typically weak and detection of optical signals in dense tissues is hampered by light attenuation and scattering (22, 25). We developed an approach to augment cellular promoter activity and light output based on a concept termed two-step transcriptional amplification or

TSTA (26, 27). In the original TSTA scheme, a cellular promoter expresses a potent chimeric activator, GAL4-VP16. GAL4-VP16 is a fusion of the high affinity yeast GAL4 DNA binding domain to the potent Herpes Simplex virus VP16 activation domain (28, 29). GAL4-VP16 binds a GAL4-responsive reporter gene and generates high levels of FLuc. Our PCa-specific version of the TSTA system employs a modified PSA promoter, which responds more robustly than the native promoter to the AR (30). It also contains a more potent derivative of GAL4-VP16, where the VP16 activation domain is dimerized (GAL4-VP2).

We previously employed this optimized AR-responsive TSTA vector to generate adenovirus (AdTSTA), lentivirus (LentiTSTA) and transgenic animals, which were employed to sensitively measure AR signaling in xenograft tumors or native prostate tissue of mice (26, 27, 31). An advantage of the AdTSTA approach is the ability to inject the virus into any tumor in any xenograft animal. Many of the xenografts do not exist as cell lines, placing a limitation on the development of stably transformed cells.

To detect MAPK in a prostate specific manner we took advantage of the binary design of TSTA to craft an imaging cassette that simultaneously measures AR and MAPK function. The principle is illustrated in Figure 1A. In the first step, a modified PSA regulatory region expresses GAL4-ELK1, rather than GAL4-VP16. GAL4-ELK1 contains the GAL4 DNA binding

domain fused to the activation domain of ELK1 (32). Phosphorylation of the ELK1 activation domain by ERK1/2 occurs at several serines and threonines, with phosphorylation of S383 being the most important since its mutation disables ELK1-mediated activation (32, 33). Phospho-ELK1 recruits the Mediator co-activator complex (34) and stimulates transcription from a GAL4-responsive reporter gene expressing FLuc. The FLuc bioluminescent activity is detected using the Xenogen IVIS.

Our previous studies have shown that the amount of luciferase activity is proportional to the activity of AR both *in vitro* and in animals (19, 27). Further, the AdTSTA approach was highly successful in quantifying AR function in response to androgen deprivation and anti-androgen therapy (19, 35). The system is tissue specific and detects FLuc only in prostate when inserted into transgenic animals (31). Based on these results we surmised that the TSTA-ELK1 system would be able to detect combined effect of AR and MAPK on transcription in living animals. We emphasize that by using the GAL4-ELK1 system we measure functional MAPK activity through a reporter gene readout.

Our study was designed to address three key questions: 1. Will TSTA-ELK1 detect MAPK signals in cell culture and in live animals? 2. Do AI tumors display higher levels of MAPK than AD tumors? 3. Do different xenograft models display the same functional basal levels of MAPK?

We found that the TSTA-ELK1 system functioned in cell culture in response to MAPK and AR stimulants. When an adenovirus encoding the TSTA-ELK1 cassette was injected into tumors it detected increased MAPK activity in response to systemic injection of EGF. Surprisingly, the AdTSTA-ELK1 system detected similar levels of MAPK in both the AI and AD forms of PCa. However, the basal AdTSTA-ELK1 activities differed significantly (>100-fold) between two different xenograft models of PCa, CWR22 and LAPC9. We discuss the applications and limitations of our approach in understanding the role of MAPK in PCa.

RESULTS

TSTA-ELK1 Detects MAPK in Cell Culture

Figure 1B shows that the TSTA-ELK1 system functions in a simple transfection experiment performed in LNCaP cells. A plasmid bearing the TSTA-ELK1 system was transfected with combinations of R1881, an androgen agonist, and another plasmid encoding a dominant active form of MEKK (DA-MEKK), a kinase molecule upstream of ERK1/2 in the RAS-MAPK signaling cascade. Modest increases in FLuc reporter gene activity were observed with DA-MEKK and R1881 alone. The combination of DA-MEKK and R1881 led to a synergistic increase in FLuc expression. The fact that low level expression is observed with R1881 and DA-MEKK alone

is consistent with previous reports showing that androgens can activate the MAPK pathway through a non-genotropic signaling mechanism (15-17) and DA-MEKK can facilitate AR function in the presence of only trace, castrate levels of androgen (36). Figure 1C shows an immunoblot confirming that GAL4-ELK1 expression is detected at a low level in the absence of R1881. This low level expression is likely due to the potency of the modified PSA enhancer (30). We previously reported that the TSTA vector can utilize trace amounts of DHT remaining in charcoal depleted serum and the anti-androgen bicalutamide is necessary to completely ablate GAL4 expression in cell culture (27). Nevertheless, GAL4-ELK1 expression is increased significantly by R1881 and by the combination of R1881 and DA-MEKK but not by DA-MEKK alone.

As described in the Introduction there have been many studies that support some form of crosstalk between the AR and MAPK pathways (1, 6). MAPK has been shown to stimulate AR activity in a variety of different contexts (10, 13, 14, 36-38). To further validate and characterize the TSTA-ELK1 system, which measures the combined action of MAPK and AR, we compared it to the original TSTA system, which is mainly AR-responsive. Figure 2A shows that the TSTA-ELK1 reporter response is synergistic when transfected into LNCaP cells treated with a combination of R1881 and EGF. Furthermore, specific inhibitors of the EGF receptor

tyrosine kinase and AR, PKI-166 (13, 39) and casodex (also called bicalutamide), respectively, eliminate the synergistic response. Figure 2B shows a similar experiment with the TSTA system. In this example, EGF alone stimulates a mild increase in AR activity but R1881 strongly stimulates activity. The TSTA reporter response is strongly inhibited by casodex and only marginally inhibited by PKI166 (lanes 5-10). The inhibition by PKI166 of basal AR activity confirms previous reports that EGF or HER2 affects AR activity although the effect, under the conditions employed here, is not as dramatic as optimized conditions reported by others (14). Although the TSTA system does respond to EGF and its inhibitors, the effects are less than 2-fold and significantly less than the strong synergy observed with R1881 and EGF in the TSTA-ELK1 system. For example, the difference between R1881 alone and R1881 plus EGF is only 1.5 fold with TSTA versus 25-fold with TSTA-ELK1. We conclude that the TSTA-ELK1 system is more specific and appropriate for studying the MAPK response in PCa than the original TSTA system.

Detecting EGF-activated MAPK in Xenografts

To evaluate functional MAPK levels in xenograft models of PCa we generated a replication defective adenovirus bearing the TSTA-ELK1 cassette. Figure 3A illustrates the structure of AdTSTA-ELK1, where a

duplicated PSA enhancer, attached to the PSA promoter expresses GAL4-ELK1 in the rightward direction, while a GAL4-responsive FLuc reporter is oriented head-to-head in the leftward direction in an E1/E3 deleted Ad5 vector (40). The virus was amplified, titered and used for injection into xenograft models of PCa.

In Figure 3B we show a time course of FLuc expression 3-4 days after injection of AdTSTA-ELK1 into 0.5 cm tumors in the CWR22r-2524 (CWR22-AI) prostate xenograft model (41). CWR22-AI is a subclone of the CWR22 xenograft series, a human prostatic carcinoma grown on castrated male SCID mice (42). CWR22-AI expresses PSA and a mutant AR (43). A series of prior optimization experiments revealed that FLuc expression reached peak levels within 4 hours of EGF injection. This point is emphasized in the figure, where FLuc activity increases 4 hours after injection, versus a control animal, and remains high for at least 24 hours. We observe a minor elevation in activity when a second baseline measurement is taken 72 hours later followed by a dose of EGF for 4 hours.

We observed similar stimulations 4 hours post injection in the LAPC9 model. LAPC9 is derived from a bone metastasis and expresses wild-type AR and PSA (18, 44). Representative images are shown for the LAPC9 AD and AI xenograft models in Figure 3C. Figure 3D is a bar

graph averaging data from cohorts of 8 LAPC9 AD and AI animals. The blue bars represent the fold change in the vehicle- or control-treated animals and the red bars represent EGF-treated animals 4 hours after taking baseline measurements. A consistent 2- to 3.5-fold induction of FLuc expression was detected in the EGF-treated animal versus controls. We conclude that the AdTSTA-ELK1 can detect the systemic effect of EGF injection on MAPK mediated activity in tumors of live animals.

Differences between MAPK Activity in AD and AI Tumors

One of the hypotheses concerning the transition of PCa from an AD to AI state is that it is driven by RTK and downstream MAPK activity (6, 7). One prediction of that hypothesis is that the basal MAPK levels of AI tumors will greatly exceed that of AD tumors. We therefore employed the AdTSTA-ELK1 system to examine the basal levels of functional MAPK activity within xenograft tumors of live animals. We compared the levels of MAPK in both the CWR22 and LAPC9 xenografts. Figure 4A shows the optical CCD signals from representative AD and AI animals 3 days after viral injection and figure 4B graphs the results from cohorts (n=10 for AD and n=8 for AI) of animals. We illustrate the animals using the same photonic scale to illustrate the large difference between models as described below.

Two important observations emerged from this analysis. First, we found only marginal differences between the AD and AI tumors within each xenograft model. This suggests that MAPK levels do not change significantly when the tumor transitions into the AI state in the xenografts. The second observation was that the AdTSTA-ELK1 activity in the CWR22 models is over 100-fold higher than the signal observed in the LAPC9 models. This latter observation suggested the possibility that the xenograft models display vastly different levels of functional MAPK. This explanation, however, required further validation.

We considered the possibility that the CWR22 AD and AI tumors grew at a significantly different rate versus LAPC9. MAPK levels are known to be elevated in highly proliferating cells (45). However, when the growth rates (n=5) of LAPC9 and CWR22 AD and AI xenografts were measured we found no correlation between functional MAPK and the growth (data not shown).

Another possibility was that the differences in AdTSTA-ELK1 activity derive from differences in the functional AR activity or infectivity of the adenovirus in the different xenograft models. To address these issues we injected cohorts of LAPC9 and CWR22 AD and AI xenografts with low levels of AdTSTA. As described above, AdTSTA expresses GAL4-VP16 from a modified PSA enhancer and measures the AR responsiveness of a

prostate tumor. The bar graph in Figure 5 compares the ratio of the AdTSTA activity in LAPC9 versus CWR22 AD and AI tumors (gray bars) against the AdTSTA-ELK1 activities (black bars). The data show that CWR22 xenografts display higher functional AR activity. The differences average 8 fold for the AD xenografts and 11 fold for the AI xenografts. However, when the AdTSTA-ELK1 ratios are compared there is a 157-fold difference between the CWR22 and LAPC9 AD xenografts and a 117-fold difference between the AI xenografts. Thus, after dividing the AdTSTA-ELK1 fold differences by the AdTSTA values there remains a 20-fold difference between the AdTSTA-ELK1 and AdTSTA activity in AD tumors and a 10-fold difference in AI tumors that cannot be accounted for on the basis of AR activity or differential infectivity. We suggest that this difference is due to the MAPK activity in the xenografts.

Comparison of MAPK Levels in the Xenografts by Immunoblotting

To understand the consequences of the enhanced functional MAPK levels we performed immunoblotting analysis of the tumors from sacrificed animals (Figure 6). We prepared tumor extracts by mincing the tissue and heating it in SDS-containing buffer followed by immunoblot using antibodies to AR, PSA, ERK, phospho-ERK and β-actin. We carefully normalized the protein levels in each extract using protein assays and

Coomassie-stained SDS-gels. We further normalized the loading to the overall β-actin and ERK levels of the tumor. We show two representative samples from the CWR22 and LAPC9 AD and AI models although they are representative of numerous independent tumor isolates.

There are several important observations that bear mentioning. The overall ERK1 levels are similar between the LAPC9 and CWR22 AD and AI xenografts when normalized to protein concentration in the tumor extracts. However, phospho-ERK levels are at >6-fold higher in CWR22 versus the LAPC9 models as determined by densitometry of the autoradiographs. Thus, we surmise that the enhanced AdTSTA-ELK1 imaging activity is due in part to enhanced phospho-MAPK environment in the xenografts.

Surprisingly, the PSA levels between the xenografts also varied. The levels in CWR22 tumors AD and AI were similar but approximately 3.4 and 4.6 fold higher respectively, than their LAPC9 counterparts. This latter observation correlates roughly with the AdTSTA imaging data, where the differences were 11 and 8 fold. Thus, it is likely that the differences between the CWR and LAPC9 xenografts represent a combination of both increased AR and MAPK function.

Remarkably, the AR levels in the xenografts were also different. LAPC9 AD and AI tumors displayed approximately equal levels of AR but

they were 1.5 fold higher than those found in the CWR22 AD model. Equally surprising was the finding that CWR22 AD tumors displayed higher levels than AI tumors. Although AR and MAPK are proposed to be central molecules in PCa growth, we found no tight correlation between either or between PSA expression and tumor growth rate. Taken together with the imaging data our study suggests some surprising properties of PCa xenografts that illustrate the heterogeneity of different tumors.

DISCUSSION

The use of bioluminescence imaging of live animals is an emerging paradigm for tumor studies in preclinical models of cancer. An important application of this technology is to evaluate signaling pathways in a tissue-specific manner within a living subject. The ERK1/2 branch of the MAPK pathway is one of the major signaling pathways hypothesized to be operational in cancer. The goal of our study was to develop an imaging system that could quantitate MAPK in PCa tumors. We developed a MAPK imaging system by modifying the TSTA paradigm that we developed several years ago (26, 27, 30). We employed a modified version of the AR-responsive and prostate-specific PSA gene enhancer to express GAL4-ELK1, which then activates FLuc expression only when it is phosphorylated by MAPK. Thus, the system is specific to prostate tissue and MAPK simultaneously. The TSTA-ELK1 system represents the first generation of binary TSTA systems that can be employed to interrogate signaling pathways in a tissue-specific manner. GAL4-ELK1 is also a potent activator so that the signal is easily measurable using the current CCD imaging methodology.

Our cell culture data demonstrated that the system responds synergistically to the combined action of AR and MAPK using either artificial (DA-MEKK) or natural stimulants (EGF) of the MAPK pathway. We further showed that the system, when transferred into an adenovirus, could reproducibly measure the response to systemic EGF stimulation in the tumor of a live animal. We found that the ability to respond to EGF is a general property of AD and AI tumors from the LAPC9 and CWR22 xenograft models.

We then employed the system to address whether MAPK activity is typically elevated upon transition of a tumor from the AD to AI states. This idea has been widely explored in the literature (12, 13). We addressed this issue in two widely studied animal xenograft models of human PCa, CWR22 and LAPC9. We chose two models to evaluate the possibility that different xenograft models might display differential responses. The data strongly suggest that within a model system the AD and AI tumors display nearly identical functional MAPK activities.

Numerous studies have shown that stimulants of the MAPK response can facilitate AR activity at castrate levels of ligand both in culture and in animal models. Indeed elevated phospho-ERK levels are observed in clinical samples of patients with metastatic disease, where one study showed that phospho-ERK levels corresponded with Gleason score

(9). These researchers showed that two patients who showed low MAPK levels prior to treatment exhibited higher levels of MAPK in recurrent disease.

The observation that the xenograft data differ from patient data raises a critical issue. Typically the xenograft tumors are obtained from patients who failed therapy. However, the tumors initially grew only in an AD manner when implanted into intact male SCID or Nude mice and were later trained to grow in an AI manner by passage onto castrated male mice or the flanks of female mice. Thus, the transition to an AI state in animals may not be wholly representative of the changes observed in a patient. It is plausible that the MAPK signaling pathways have already reached peak levels in the tumors during therapy. And therefore, the xenografts may have already changed in a fundamental manner that does not fully recapitulate disease progression in a patient. Nevertheless, the xenograft tumors undergo many steps that resemble the disease in humans including slowing or cessation of growth upon castration of mice bearing AD tumors and a lowering of PSA values followed by elevation of PSA levels as the tumor transitions to the recurrent phase. It will be important to consider these issues when interpreting data from xenograft models.

Nevertheless, one surprising difference between the CWR22 and LAPC9 models is the significant increase in functional MAPK in CWR22 as

measured by imaging and whole tumor phospho-ERK levels. The phospho-ERK levels did not correlate with tumor growth rates. In fact, the two different tumor models displayed other surprising properties that point to the heterogeneity of PCa in different patients. The elevated MAPK levels were associated with higher levels of PSA in the CWR22 models versus LAPC9 but surprisingly, lower levels of AR, particularly in the CWR22 AI model. This finding was interesting because PSA is an AR-regulated gene. Numerous studies have shown that AR activity can be upregulated by stimulants of the MAPK pathway including EGF. Elevated MAPK may therefore facilitate AR function in the CWR22 versus the LAPC9 model. If this was the case then the imaging system could be used to test drugs that inhibit MAPK activity.

One other interesting finding was that AR and PSA levels are not directly correlated. The LAPC9 model displayed consistently higher AR levels but lower PSA values. Indeed, the PSA values of the AI model were slightly lower than the AD models despite nearly identical AR levels. Similarly, the CWR22 AI models show lower levels of AR versus the AD models despite the observation that PSA levels are similar. It is clear that other changes must contribute to the AI phenotype and other pathways (i.e., Akt) should eventually be interrogated. Nevertheless, the data imply

that a complex set of changes characterize PCa and even in these widely studied models no single identifiable factor dominates.

The observation that LAPC9 AD and AI display similar levels of AR contradicts a recent report claiming that the AI model displays significantly higher AR levels (46). Elevated AR is sometimes associated with AI cancer. The original reports on human clinical specimens showed that an amplified AR gene was associated with recurrent PCa (47-49). This observation has been reinforced by gene expression micro-array data and AR overexpression data (46, 50). However, our studies suggest that elevation of AR is not a mandatory feature of the AD-AI transition in animal models. It is plausible that the models evolve differently depending upon the number of xenograft passages and the manner in which the AD state is maintained. For example, our lab does not grow AD tumors in mice supplemented with slow release DHT pellets. This method is a popular approach for maintaining AD xenografts but the supra-physiological levels of DHT in such models may alter AR expression such that changes in AR levels are necessary for subsequent growth in castrate mice. We have previously shown that changes, which typically accompany castration (lower AR, PSA, slower tumor growth rates, loss of AR nuclear localization and loss of binding to the PSA gene by chromatin immunoprecipitation assays), occur in LAPC9 animal models maintained in the absence of DHT or testosterone supplements (19). Thus, even when AR levels remain

similar the tumors are able to reproduce several important aspects of the AD to AI transition.

In summary, as argued above, no single identifiable factor is characteristic of the AD to AI transition when comparing CWR and LAPC9 models. These well-studied models display differences in MAPK, PSA and AR levels yet grow similarly in castrate mice. A complex interplay contributes to PCa including AR levels (46, 48, 49, 51), the activity of various signaling pathways (12, 39, 52-54), the ability of the tumor to convert adrenal androgen to DHT, (55), plus the unknown but widely studied contribution of co-activators and co-repressors (14, 56-59).

MATERIALS AND METHODS

Plasmid and Adenoviral Constructs

The plasmid construct TSTA-ELK1 was generated from the optimal TSTA plasmid (27). In the original TSTA plasmid vector a 5' NotI site was removed to create a unique site within the vector. We recreated the 5' *Not*I site by subcloning an *Mlu*I-*Not*I polylinker into an *Mlu*I-cleaved TSTA plasmid backbone. The 8.7 Kb TSTA plasmid was then cleaved at the *Xho*I and *Not*I sites to remove the GAL4-VP16 cassette from the imaging construct. A *Xho*I-*Not*I GAL4-ELK1 fragment derived from pFA2-ELK1 (Stratagene) was subcloned into the TSTA *Xho*I-*Not*I parental plasmid resulting in generation of a single 8.7-Kb vector termed the TSTA-ELK1 plasmid. The *Not*I-*Sal*I fragment from TSTA-ELK1 was subsequently inserted into the *Not*I-*Sal*I site of pShuttle (QBiogene, Carlsbad, CA). The TSTA-ELK1 fragment was then incorporated into the adenovirus vector AdEASY (#AES1000A, QBiogene) through homologous recombination. The virus was scaled up, purified via a CsCl gradient, and tittered using the Adeno-X Rapid Titer Kit (#PT3651-2, Clonetech) following infection of 293 monolayers (infectious units = plaque forming units). Virus was stored at –80°C at 10^{10} pfus/mL in 10 mM Tris-HCl, 1 mM MgCl2, and 10% glycerol.

Cell Culture Transfection Experiments

The human PCa cell line LNCaP was grown in RPMI 1640 supplemented with 10% fetal bovine serum (FBS) and 1% penicillin/streptomycin solution (GIBCO, Mediatech). Prior to transfection, the cells were transferred into media containing 5% charcoal stripped serum (Omega Science, Tarzana, CA) for 24hrs. On day 1, we plated LNCaP cells in 6-well plates in RPMI 1640 containing charcoal-stripped FBS. We performed transient transfections 24 hours later using TFX-50 (Promega) with a lipid:DNA ratio of 4:1. Each transfection mixture contained 0.5 μg of the imaging construct and 0.5 μg of carrier DNA pGL3B (Promega). Stimulants used in the cell culture experiments were methylenetrienolone (R1881, NEN Life Science Products, Boston, MA), a synthetic androgen, and dominant active MEKK, DA-MEKK, (generously provided by Dr. Charles L. Sawyers, UCLA, CA) or epidermal growth factor (EGF) (Sigma). R881 was added to the medium at a concentration of 0.1 nM or 1 nM per well as noted in the figure legends. Depending on the experiment either 200 ng of DA-MEKK or 100 ng/well of EGF (Sigma) was added to the medium for 1 hour following transfection. Experiments using inhibitors PKI-166 (generously provided by Charles L. Sawyers, UCLA), a RTK small molecule inhibitor (13, 39) and casodex, an anti-androgen drug

were treated along side stimulants R1881 and EGF to determine inhibitory effect to TSTA and TSTA-ELK1 systems. PKI-166 was administered at 5 μM and casodex at 10 μM. Cells were then incubated at 37°C for 48 hours. The cells were harvested and lysed using the passive lysis buffer provided in the assay kit for measuring firefly luciferase (FLuc) activities (Dual-Luciferase Assay System, Promega). FLuc activities of 5% of the cell lysates with 100 μL of substrate D-luciferin were measured using a luminometer (Lumat 9507, Berthod, Germany) with an integration time of 20 seconds.

Animal CCD Experiments

The imaging was performed essentially as we described previously (19, 27). Animal care and euthanasia were performed with full approval of the University of California Animal Research Committee (ARC). For LAPC9 and CWR22 xenografts, a total of 10^7 pfu of AdTSTA-ELK1 in 20 μL of Dulbecco's Phosphate Buffered Saline (GibcoBRL) was injected into a 0.3-0.4 cm diameter tumor at two locations. The virus was allowed to express the encoded genes and distribute throughout the tumor for 3 days before imaging. On the day of imaging mice were anesthetized with ketamine-xylazine mix (4:1). Imaging was performed using a Xenogen IVIS

100 cooled CCD camera (Xenogen Corporation, Alameda, CA). The mice were injected with 200 μL of 15 mg/ml D-Luciferin intraperitoneally for 15 minutes prior to imaging after which they were placed in a light-tight chamber. A gray-scale reference image was obtained followed by the acquisition of a bioluminescent image. The acquisition time ranged from 1 to 5 minutes. The images shown are pseudoimages of the emitted light in photons/sec/cm^2/steradian, superimposed over the gray scale photographs of the animal. Time courses were performed where mice were imaged every 3 days. Because adenoviral injection delivers slightly different amounts of vector to the tumors due to viral leakage, we obtained a baseline image 3 days after viral injection and measured the percent change in signal over time. Following taking a baseline image, a subset of mice were treated with 500 μL of 100 ng/ml of EGF that dissolved in 10 mM acetic acid containing 0.1% BSA. EGF treated mice were then imaged 4 hours later to determine AdTSTA-ELK1 activity. The data were analyzed statistically using the Student's t test.

Immunoblots

For cell culture analysis, LNCaP cells were grown in 6-well plates, transfected with TSTA-ELK1 and treated with mitogens. We harvested and lysed the treated cells using RIPA lysis buffer (10 mM Tris-HCl, 150 mM

NaCl, 0.1% DOC, 1 mM EDTA, and 1% NP40). We normalized extracts by protein concentration (BCA Protein Assay Kit, Pierce) and the samples were fractionated on 4-15% gradient acrylamide gels (Bio-Rad) and subjected to immunoblot analysis with rabbit polyclonal antibodies generated against GAL4 (60, 61). For whole tumors analysis, tumors were harvested from mice via surgical resection at the imaging endpoints and immediately frozen in liquid N_2. Frozen tumors were homogenized using a mortar and pestle in the presence of liquid N_2. Samples were then resuspended in 400-600 µL RIPA buffer (10 mM Tris-HCl, 1 % NP-40, 1% Na-deoxycholate, 150 mM NaCl, 1 mM EDTA, 0.2% SDS, 1 mM PMSF, 1 µg/ml Leupeptin and Pepstatin, 1 mM Na_3VO_4, 1 mM NaF). Lysates were passed through $25^{5/8}$ gauge needles to shear genomic DNA followed by heating at 65•C and centrifugation at 14K at 4°C for 20 minutes to remove insoluble debris. Samples were assayed for total protein concentration using the Pierce BCA™ Protein Assay Kit (Catalog # 23227,23225). Extracts were fractionated on 4-15% Tris-HCl Ready Gels (Bio-Rad, Hercules, CA) and immunoblotted. After a second round of normalization using using_β-actin and ERK, blots were probed with antibodies against AR M-441 (#sc-7305) and ERK (#sc-93) were obtained from Santa Cruz, PSA (#A0562) from DAKO Corporation, phosphorylated p44/p42

ERK/MAPK (#E10) from Cell Signaling Technology, and β-actin (#A5441) from Sigma.

LEGENDS

FIG. 1. The TSTA-ELK1 Prostate and MAPK Specific Imaging Construct. A) Depiction of the two-step transcriptional activation process. In the first-step, the modified PSA enhancer present within the effector cassette of the imaging construct activates expression of the GAL4-ELK1 derivatives (ovals) in PCa cells. In the second-step, the GAL4-ELK1 fusion protein is activated by phosphorylation of MAPK(ERK1/2). The GAL4-ELK1 fusion protein binds to a GAL4-responsive promoter in the reporter cassette and activates expression of firefly luciferase. B) Validation of TSTA-ELK1 response to AR and MAPK pathways in cultured cells. LNCaP cells grown in 6-well plates were transiently transfected with TSTA-ELK1 plasmid. We added 10 nM R1881 (synthetic androgen) and dominant active MEKK (DA-MEKK), together or separately, to samples 1 hour after transfection and measured the luciferase activity 48 hours after stimulation. These experiments were repeated multiple times in triplicate. The measurements shown here are average values of a representative experiment. The vertical axis shows the relative light unit reading from the luminometer. The

error bars represent standard deviation. C) Below the graph is an immunoblot showing LNCaP cell extracts probed with GAL4 antibodies to detect GAL4-ELK1 expression.

FIG 2. Specificity of the TSTA-ELK1 and TSTA Imaging Constructs. A) FLuc assay of LNCaP cells transiently transfected with TSTA-ELK1 plasmid. Cells were treated together or separately with 0.1 nM R1881 (R) and 100 ng of recombinant epidermal growth factor (E) and with or without inhibitors PKI-166 (PKI), an EGF/HER2 RTK inhibitor, and casodex (Cas), an anti-androgen. Cell lysates were assayed for FLuc activity 48 hours after treatment using a luminometer. Assays were done in triplicate and representative FLuc assay is shown. B) FLuc assay of LNCaP cells transiently transfected with TSTA. Cells were treated together or separately with 0.1nM R1881 and 100 ng EGF with or without PKI-166 and casodex. Cells were lysed and processed for FLuc analysis after 48 hours. Cell culture experiments were performed multiple times in triplicate. A representative experiment is shown. Error bars represent the standard deviation.

FIG 3. AdTSTA-ELK1 Monitors Both AR and MAPK Activity *In vivo*. A) Schematic representation of the AdTSTA-ELK1 vector. AdTSTA-ELK1 was constructed using a modified form of the AdTSTA system (27). B) Time course of AdTSTA-ELK1 signaling in CWR22-25/24 androgen independent xenograft model. Mice were baseline imaged 3 days following AdTSTA-ELK1 injection and then treated with exogenous EGF intraperitoneally. We allowed 4 hours of incubation for EGF to stimulate the MAPK pathway in the tumor and then re-imaged in the IVIS CCD camera. Acquisition time of imaging was 3 to 5 minutes. Following 72 hours of rest, the mice were again baseline imaged and then received EGF as noted above. Representative control and EGF treated mice are shown. C) Imaging AR and MAPK signaling in the LAPC9 PCa xenograft model. Castrated (AI) or intact (AD) male SCID mice implanted subcutaneous with LAPC9 tumors (0.5cm) and were injected intratumorally with 2e+7 pfus of AdTSTA-ELK1. After 3 days mice were injected intraperitoneally with of EGF or vehicle control and then imaged 4 hours later to evaluate MAPK activation. Representative mice are shown post 4 hours EGF treatment. D) Bar graph summarizes several experiments with cohorts of n=8 of LAPC9-AD and n=8 LAPC9–AI xenografts injected with AdTSTA-ELK1. Graph depicts the fold change of signal of AdTSTA-ELK1 activity post-EGF treatment. Error bars indicate standard deviation.

FIG 4. Comparison of the Basal Activities of LAPC9 and CWR22 Xenografts. A) LAPC9 (AD, AI) and CWR22 (AD, AI) xenografts were injected intratumorally with 4.7e+07 pfu of AdTSTA-ELK1. Pseudoimages were normalized to the CWR22 xenograft images to demonstrate the difference in signals between the two PCa xenografts. B) Bar graph summarizing the average basal signal of the two PCa xenografts in photons/second/cm^2/steridian. Graph depicts the average basal level signals on day 3 following injection of virus.

FIG 5. Comparing the MAPK Specificity of AdTSTA-ELK1 and AdTSTA in the LAPC9 and CWR22 Xenograft Models. AdTSTA-ELK1 and AdTSTA were injected into LAPC9 or CWR22 xenografts when tumors reached <0.5 cm in diameter. Baseline signals of each imaging construct were taken 3 days post injection of the viral vector. Graph depicts the fold difference in activity of each imaging construct in the each xenograft model (LAPC9 vs. CWR22) and each model type (AD vs. AI).

FIG 6. Molecular Differences in the LAPC9 and CWR22 Xenograft Models. Western blot analysis of AR, PSA, phospho-ERK1/2 (p42/44) and ERK1 (p44) expression from harvested and extracted xenografts. Total protein

was extracted from tumors and immunoblotting was performed using specific antibodies against each protein. β-actin and ERK were used to normalize loading of the extracts onto the gels for the final immunoblot. Lanes 1, 2, 5 and 6 depict independent isolates of androgen dependent (AD) tumor samples from LAPC9 (lanes 1 and 2) and CWR22 tumors (lanes 5 and 6). Lanes 3, 4, 7, and 8 depict separate androgen independent (AI) tumor samples from LAPC9 (lanes 3 and 4) and CWR22 (lanes 7 and 8) tumors.

REFERENCES

1. Gioeli, D. Signal transduction in prostate cancer progression. Clin Sci (Lond) 2005;*108:* 293-308.
2. Martin, G. S. Cell signaling and cancer. Cancer Cell 2003;*4:* 167-174.
3. Buchwalter, G., Gross, C., and Wasylyk, B. Ets ternary complex transcription factors. Gene 2004;*324:* 1-14.
4. Heinlein, C. A. and Chang, C. Androgen receptor in prostate cancer. Endocr Rev 2004;*25:* 276-308.
5. Gelmann, E. P. Molecular biology of the androgen receptor. J Clin Oncol 2002;*20:* 3001-3015.
6. Culig, Z. Androgen receptor cross-talk with cell signalling pathways. Growth Factors 2004;*22:* 179-184.
7. Weber, M. J. and Gioeli, D. Ras signaling in prostate cancer progression. J Cell Biochem 2004;*91:* 13-25.
8. Feldman, B. J. and Feldman, D. The development of androgen-independent prostate cancer. Nat Rev Cancer 2001;*1:* 34-45.
9. Gioeli, D., Mandell, J. W., Petroni, G. R., Frierson, H. F., Jr., and Weber, M. J. Activation of mitogen-activated protein kinase associated with prostate cancer progression. Cancer Res 1999;*59:* 279-284.
10. Yeh, S. Y., Lin, H. K., Kang, H. Y., Thin, T. H., Lin, M. F., and Chang, C. S. From HER2/Neu signal cascade to androgen receptor and its coactivators: A novel pathway by induction of androgen target genes through MAP kinase in prostate cancer cells. Proceedings of the National Academy of Sciences of the United States of America 1999;*96:* 5458-5463.
11. Slamon, D. J., Godolphin, W., Jones, L. A., Holt, J. A., Wong, S. G., Keith, D. E., Levin, W. J., Stuart, S. G., Udove, J., Ullrich, A., and et al. Studies of the HER-2/neu proto-oncogene in human breast and ovarian cancer. Science 1989;*244:* 707-712.
12. Craft, N., Shostak, Y., Carey, M., and Sawyers, C. A mechanism for hormone-independent prostate cancer through modulation of androgen receptor signaling by the HER-2/neu tyrosine kinase. Nature Medicine 1999;*5:* 280-285.
13. Mellinghoff, I. K., Tran, C., and Sawyers, C. L. Growth Inhibitory Effects of the Dual ErbB1/ErbB2 Tyrosine Kinase Inhibitor PKI-166 on Human Prostate Cancer Xenografts. Cancer Res 2002;*62:* 5254-5259.
14. Gregory, C. W., Fei, X., Ponguta, L. A., He, B., Bill, H. M., French, F. S., and Wilson, E. M. Epidermal growth factor increases coactivation of the androgen receptor in recurrent prostate cancer. J Biol Chem 2004;*279:* 7119-7130.

15. Heinlein, C. A. and Chang, C. The roles of androgen receptors and androgen-binding proteins in nongenomic androgen actions. Mol Endocrinol 2002;*16:* 2181-2187.
16. Migliaccio, A., Castoria, G., Di Domenico, M., de Falco, A., Bilancio, A., Lombardi, M., Barone, M. V., Ametrano, D., Zannini, M. S., Abbondanza, C., and Auricchio, F. Steroid-induced androgen receptor-oestradiol receptor beta-Src complex triggers prostate cancer cell proliferation. Embo J 2000;*19:* 5406-5417.
17. Kousteni, S., Bellido, T., Plotkin, L. I., O'Brien, C. A., Bodenner, D. L., Han, L., Han, K., DiGregorio, G. B., Katzenellenbogen, J. A., Katzenellenbogen, B. S., Roberson, P. K., Weinstein, R. S., Jilka, R. L., and Manolagas, S. C. Nongenotropic, sex-nonspecific signaling through the estrogen or androgen receptors: dissociation from transcriptional activity. Cell 2001;*104:* 719-730.
18. Klein, K. A., Reiter, R. E., Redula, J., Moradi, H., Zhu, X. L., Brothman, A. R., Lamb, D. J., Marcelli, M., Belldegrun, A., Witte, O. N., and Sawyers, C. L. Progression of metastatic human prostate cancer to androgen independence in immunodeficient SCID mice. Nat Med 1997;*3:* 402-408.
19. Zhang, L., Johnson, M., Le, K. H., Sato, M., Ilagan, R., Iyer, M., Gambhir, S. S., Wu, L., and Carey, M. Interrogating androgen receptor function in recurrent prostate cancer. Cancer Res 2003;*63:* 4552-4560.
20. Blasberg, R. G. Molecular imaging and cancer. Mol Cancer Ther 2003;*2:* 335-343.
21. Choy, G., Choyke, P., and Libutti, S. K. Current advances in molecular imaging: noninvasive in vivo bioluminescent and fluorescent optical imaging in cancer research. Mol Imaging 2003;*2:* 303-312.
22. Massoud, T. F. and Gambhir, S. S. Molecular imaging in living subjects: seeing fundamental biological processes in a new light. Genes Dev 2003;*17:* 545-580.
23. McCaffrey, A., Kay, M. A., and Contag, C. H. Advancing molecular therapies through in vivo bioluminescent imaging. Mol Imaging 2003;*2:* 75-86.
24. Bhaumik, S., Lewis, X. Z., and Gambhir, S. S. Optical imaging of Renilla luciferase, synthetic Renilla luciferase, and firefly luciferase reporter gene expression in living mice. J Biomed Opt 2004;*9:* 578-586.
25. Herschman, H. R. Molecular imaging: looking at problems, seeing solutions. Science 2003;*302:* 605-608.
26. Iyer, M., Wu, L., Carey, M., Wang, Y., Smallwood, A., and Gambhir, S. S. Two-step transcriptional amplification as a method for imaging reporter gene expression using weak promoters. Proc. Natl. Acad. Sci. U S A 2001;*98:* 14595-14600.

27. Zhang, L., Adams, J. Y., Billick, E., Ilagan, R., Iyer, M., Le, K., Smallwood, A., Gambhir, S. S., Carey, M., and Wu, L. Molecular engineering of a two-step transcription amplification (TSTA) system for transgene delivery in prostate cancer. Mol Ther 2002;*5:* 223-232.
28. Emami, K. H. and Carey, M. A synergistic increase in potency of a multimerized VP16 transcriptional activation domain. Embo J 1992;*11:* 5005-5012.
29. Sadowski, I., Ma, J., Triezenberg, S., and Ptashne, M. GAL4-VP16 is an unusually potent transcriptional activator. Nature 1988;*335:* 563-564.
30. Wu, L., Matherly, J., Smallwood, A., Adams, J. Y., Billick, E., Belldegrun, A., and Carey, M. Chimeric PSA enhancers exhibit augmented activity in prostate cancer gene therapy vectors. Gene Ther 2001;*8:* 1416-1426.
31. Iyer, M., Salazar, F. B., Lewis, X., Zhang, L., Wu, L., Carey, M., and Gambhir, S. S. Non-invasive imaging of a transgenic mouse model using a prostate-specific two-step transcriptional amplification strategy. Transgenic Res 2005;*14:* 47-55.
32. Marais, R., Wynne, J., and Treisman, R. The SRF accessory protein Elk-1 contains a growth factor-regulated transcriptional activation domain. Cell 1993;*73:* 381-393.
33. Hill, C. S. and Treisman, R. Transcriptional regulation by extracellular signals: mechanisms and specificity. Cell 1995;*80:* 199-211.
34. Cantin, G. T., Stevens, J. L., and Berk, A. J. Activation domain-mediator interactions promote transcription preinitiation complex assembly on promoter DNA. Proc Natl Acad Sci U S A 2003;*100:* 12003-12008.
35. Ilagan, R., Zhang, L. J., Pottratz, J., Le, K., Salas, S., Iyer, M., Wu, L., Gambhir, S. S., and Carey, M. Imaging Androgen Receptor Function During Flutamide Treatment in the LAPC9 Xenograft Model. Molecular Cancer Therapuetics 2005;*in press.*
36. Abreu-Martin, M. T., Chari, A., Palladino, A. A., Craft, N. A., and Sawyers, C. L. Mitogen-activated protein kinase kinase kinase 1 activates androgen receptor-dependent transcription and apoptosis in prostate cancer. Molecular and Cellular Biology 1999;*19:* 5143-5154.
37. Liu, Y., Majumder, S., McCall, W., Sartor, C. I., Mohler, J. L., Gregory, C. W., Earp, H. S., and Whang, Y. E. Inhibition of HER-2/neu kinase impairs androgen receptor recruitment to the androgen responsive enhancer. Cancer Res 2005;*65:* 3404-3409.
38. Ueda, T., Bruchovsky, N., and Sadar, M. D. Activation of the androgen receptor N-terminal domain by interleukin-6 via MAPK and STAT3 signal transduction pathways. J Biol Chem 2002;*277:* 7076-7085.
39. Mellinghoff, I. K., Vivanco, I., Kwon, A., Tran, C., Wongvipat, J., and Sawyers, C. L. HER2/neu kinase-dependent modulation of androgen

receptor function through effects on DNA binding and stability. Cancer Cell 2004;*6:* 517-527.

40. He, T. C., Zhou, S., da Costa, L. T., Yu, J., Kinzler, K. W., and Vogelstein, B. A simplified system for generating recombinant adenoviruses. Proc Natl Acad Sci U S A 1998;*95:* 2509-2514.
41. Kochera, M., Depinet, T. W., Pretlow, T. P., Giaconia, J. M., Edgehouse, N. L., Pretlow, T. G., and Schwartz, S. Molecular cytogenetic studies of a serially transplanted primary prostatic carcinoma xenograft (CWR22) and four relapsed tumors. Prostate 1999;*41:* 7-11.
42. Wainstein, M. A., He, F., Robinson, D., Kung, H. J., Schwartz, S., Giaconia, J. M., Edgehouse, N. L., Pretlow, T. P., Bodner, D. R., Kursh, E. D., and et al. CWR22: androgen-dependent xenograft model derived from a primary human prostatic carcinoma. Cancer Res 1994;*54:* 6049-6052.
43. Gregory, C. W., Hamil, K. G., Kim, D., Hall, S. H., Pretlow, T. G., Mohler, J. L., and French, F. S. Androgen receptor expression in androgen-independent prostate cancer is associated with increased expression of androgen-regulated genes. Cancer Res 1998;*58:* 5718-5724.
44. Craft, N., Chhor, C., Tran, C., Belldegrun, A., DeKernion, J., Witte, O. N., Said, J., Reiter, R. E., and Sawyers, C. L. Evidence for clonal outgrowth of androgen-independent prostate cancer cells from androgen-dependent tumors through a two-step process. Cancer Res 1999;*59:* 5030-5036.
45. Sebolt-Leopold, J. S. and Herrera, R. Targeting the mitogen-activated protein kinase cascade to treat cancer. Nat Rev Cancer 2004;*4:* 937-947.
46. Chen, C. D., Welsbie, D. S., Tran, C., Baek, S. H., Chen, R., Vessella, R., Rosenfeld, M. G., and Sawyers, C. L. Molecular determinants of resistance to antiandrogen therapy. Nat Med 2004;*10:* 33-39.
47. Kim, D., Gregory, C. W., French, F. S., Smith, G. J., and Mohler, J. L. Androgen Receptor Expression and Cellular Proliferation During Transition from Androgen-Dependent to Recurrent Growth after Castration in the CWR22 Prostate Cancer Xenograft. Am J Pathol 2002;*160:* 219-226.
48. Koivisto, P., Kononen, J., Palmberg, C., Tammela, T., Hyytinen, E., Isola, J., Trapman, J., Cleutjens, K., Noordzij, A., Visakorpi, T., and Kallioniemi, O. P. Androgen receptor gene amplification: a possible molecular mechanism for androgen deprivation therapy failure in prostate cancer. Cancer Res 1997;*57:* 314-319.
49. Visakorpi, T., Hyytinen, E., Koivisto, P., Tanner, M., Keinanen, R., Palmberg, C., Palotie, A., Tammela, T., Isola, J., and Kallioniemi, O. P. In vivo amplification of the androgen receptor gene and progression of human prostate cancer. Nat Genet 1995;*9:* 401-406.

50. Sirotnak, F. M., She, Y., Khokhar, N. Z., Hayes, P., Gerald, W., and Scher, H. I. Microarray analysis of prostate cancer progression to reduced androgen dependence: studies in unique models contrasts early and late molecular events. Mol Carcinog 2004;*41:* 150-163.
51. Ford, O. H., 3rd, Gregory, C. W., Kim, D., Smitherman, A. B., and Mohler, J. L. Androgen receptor gene amplification and protein expression in recurrent prostate cancer. J Urol 2003;*170:* 1817-1821.
52. Stewart, L. V. and Weigel, N. L. Vitamin D and prostate cancer. Exp Biol Med (Maywood) 2004;*229:* 277-284.
53. Wang, S., Gao, J., Lei, Q., Rozengurt, N., Pritchard, C., Jiao, J., Thomas, G. V., Li, G., Roy-Burman, P., Nelson, P. S., Liu, X., and Wu, H. Prostate-specific deletion of the murine Pten tumor suppressor gene leads to metastatic prostate cancer. Cancer Cell 2003;*4:* 209-221.
54. Culig, Z., Hobisch, A., Cronauer, M. V., Radmayr, C., Trapman, J., Hittmair, A., Bartsch, G., and Klocker, H. Androgen receptor activation in prostatic tumor cell lines by insulin-like growth factor-I, keratinocyte growth factor, and epidermal growth factor. Cancer Res 1994;*54:* 5474-5478.
55. Mohler, J. L., Gregory, C. W., Ford, O. H., 3rd, Kim, D., Weaver, C. M., Petrusz, P., Wilson, E. M., and French, F. S. The androgen axis in recurrent prostate cancer. Clin Cancer Res 2004;*10:* 440-448.
56. Debes, J. D., Comuzzi, B., Schmidt, L. J., Dehm, S. M., Culig, Z., and Tindall, D. J. p300 regulates androgen receptor-independent expression of prostate-specific antigen in prostate cancer cells treated chronically with interleukin-6. Cancer Res 2005;*65:* 5965-5973.
57. Song, L. N., Coghlan, M., and Gelmann, E. P. Antiandrogen effects of mifepristone on coactivator and corepressor interactions with the androgen receptor. Mol Endocrinol 2004;*18:* 70-85.
58. Kang, Z., Janne, O. A., and Palvimo, J. J. Coregulator recruitment and histone modifications in transcriptional regulation by the androgen receptor. Mol Endocrinol 2004;*18:* 2633-2648.
59. Gaughan, L., Logan, I. R., Cook, S., Neal, D. E., and Robson, C. N. Tip60 and Histone Deacetylase 1 Regulate Androgen Receptor Activity through Changes to the Acetylation Status of the Receptor. J Biol Chem 2002;*277:* 25904-25913.
60. Carey, M., Leatherwood, J., and Ptashne, M. A potent GAL4 derivative activates transcription at a distance *in vitro*. Science 1990;*247:* 710-712.
61. Carey, M., Lin, Y. S., Green, M. R., and Ptashne, M. A mechanism for synergistic activation of a mammalian gene by GAL4 derivatives. Nature 1990;*345:* 361-364.

Figure 1

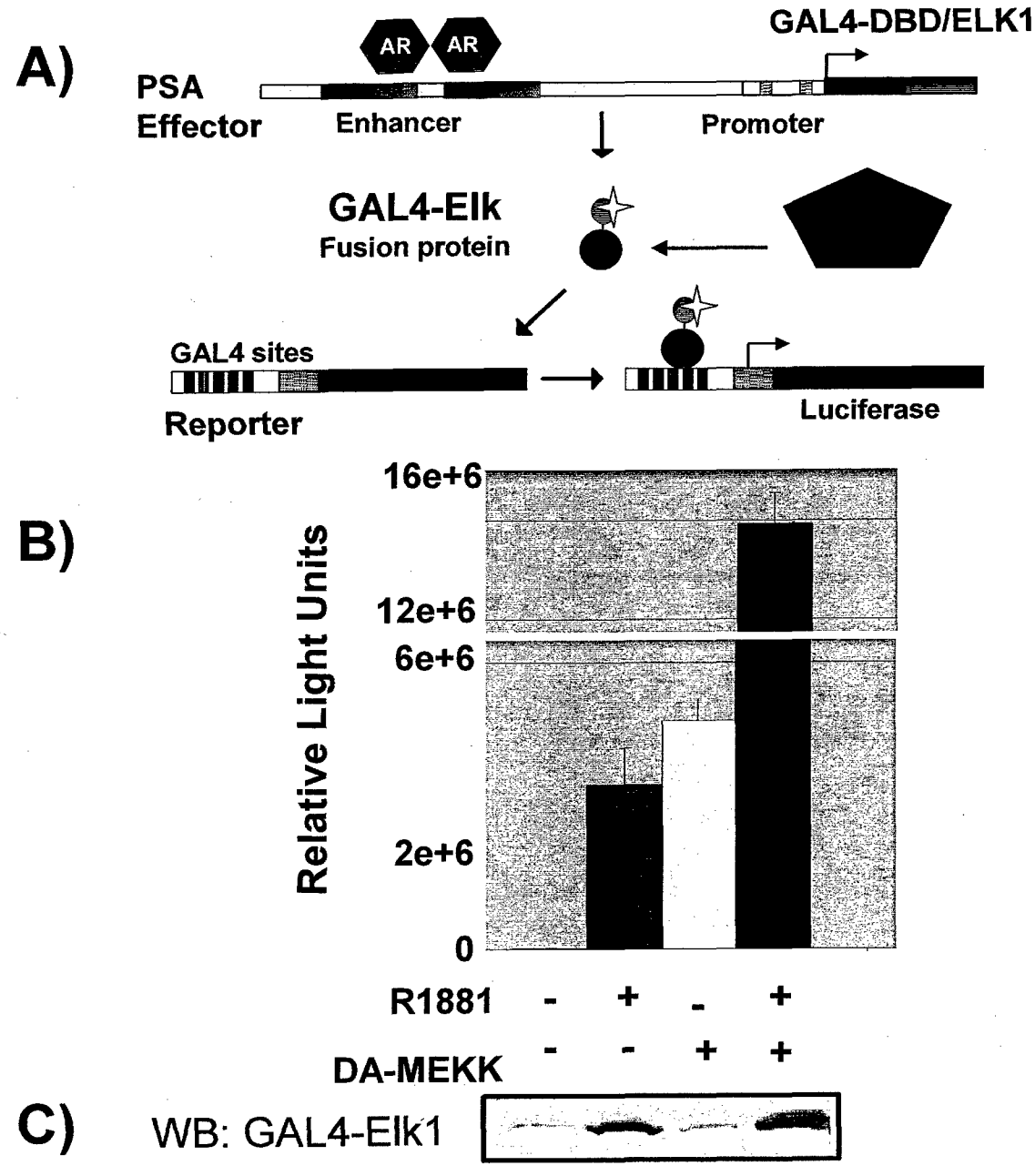
A)
AR
AR
GAL4-DBD/ELK1
PSA
Effector
Enhancer
Promoter
GAL4-Elk
Fusion protein
GAL4 sites
Reporter
Luciferase
B)
16e+6
12e+6
6e+6
2e+6
0
Relative Light Units
R1881 - + - +
DA-MEKK - - + +
C)
WB: GAL4-Elk1

Figure 2

A) TSTA-ELK

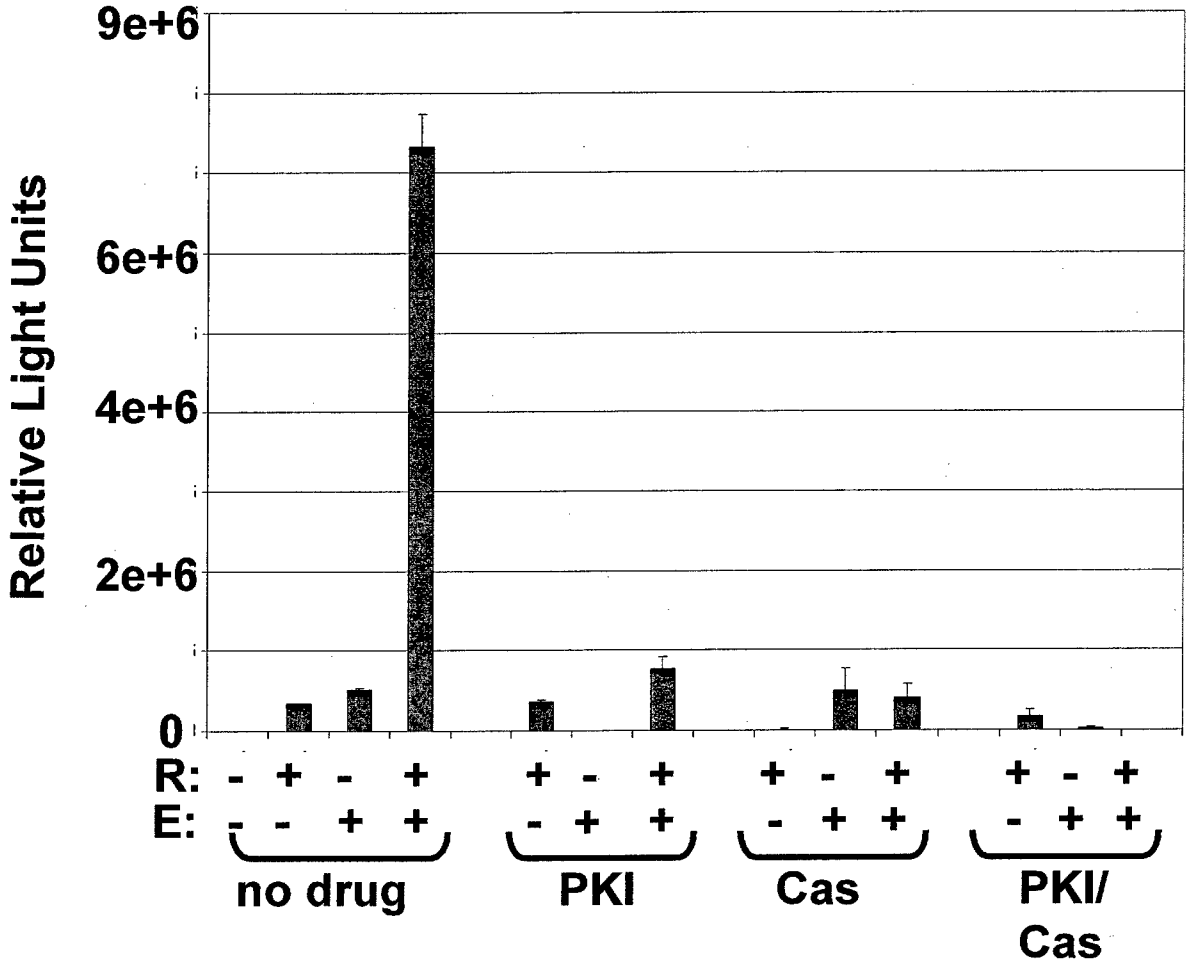

Figure 2

B) TSTA

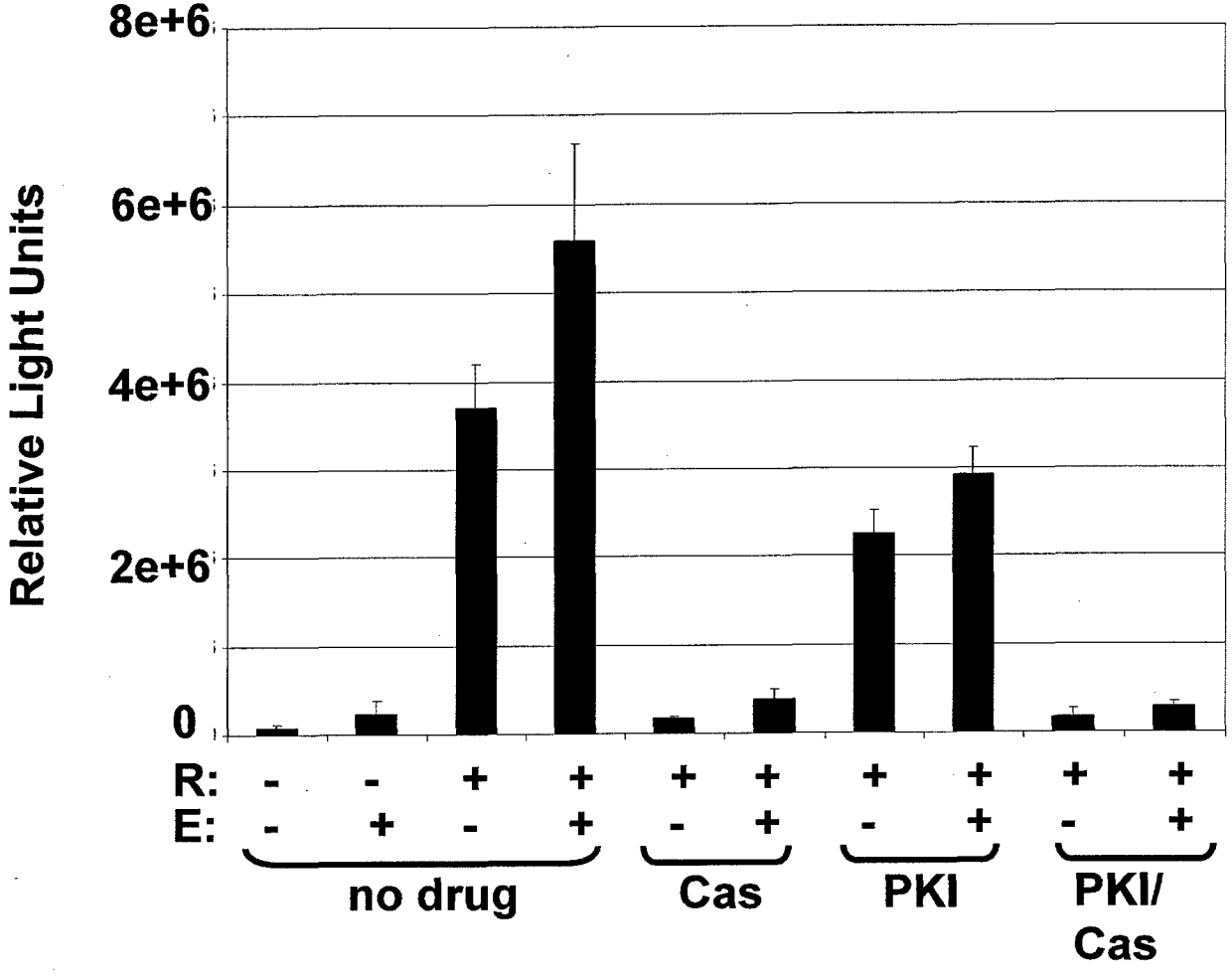

Figure 3

A)

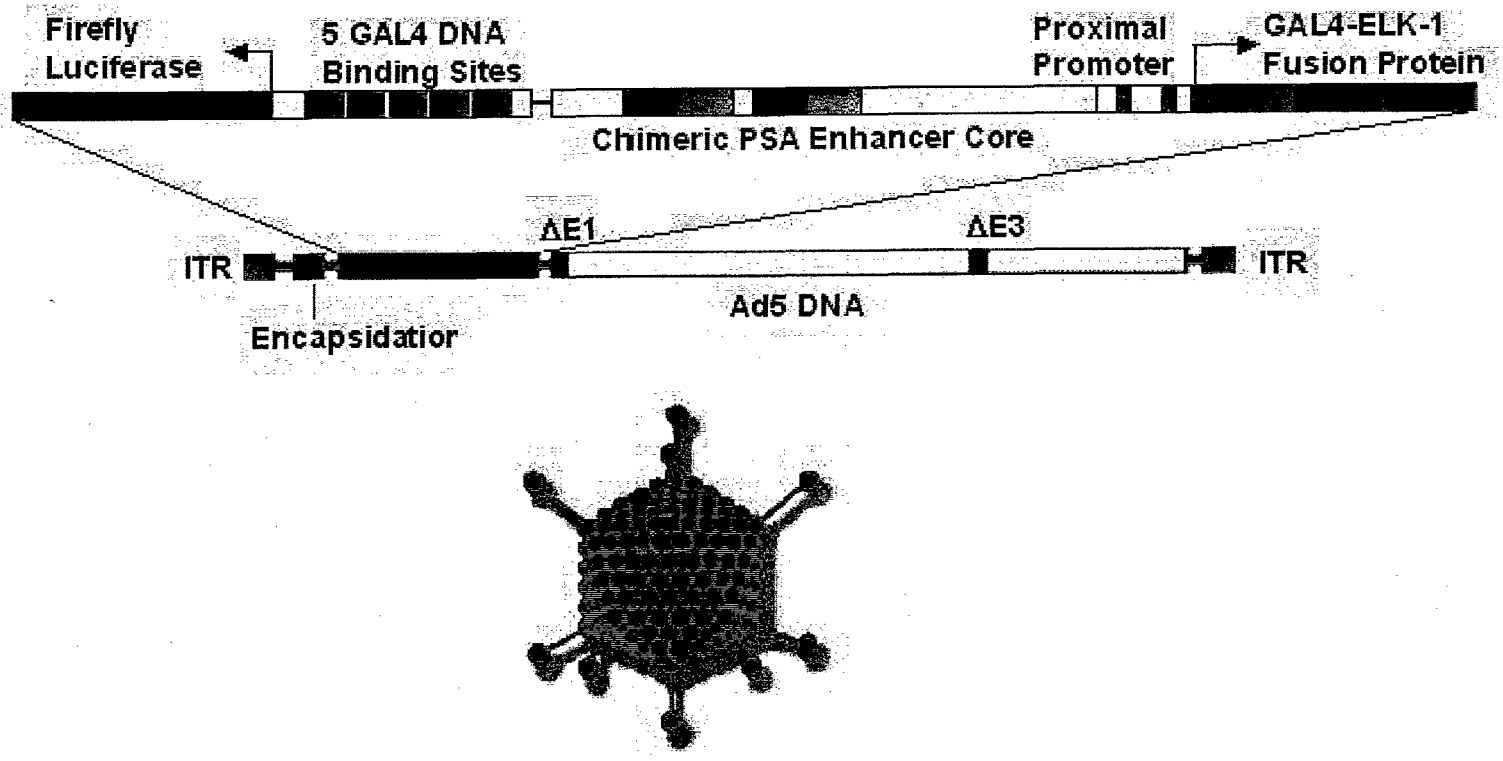
Firefly
Luciferase
5 GAL4 DNA
Binding Sites
Proximal
Promoter
GAL4-ELK-1
Fusion Protein
Chimeric PSA Enhancer Core
ΔE1
ΔE3
ITR
ITR
Ad5 DNA
Encapsidation

Figure 3

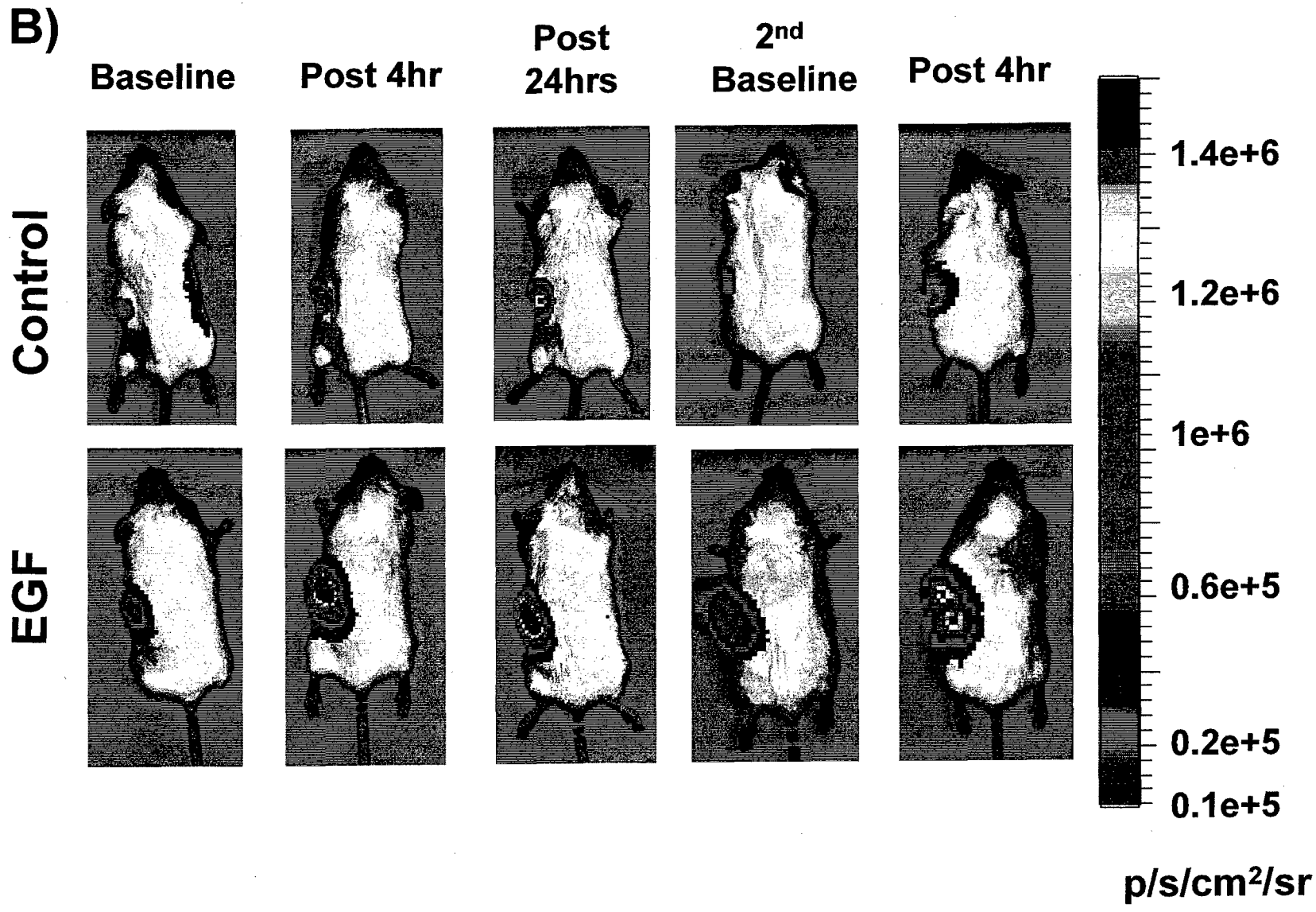
B)
Baseline
Post 4hr
Post 24hrs
2nd Baseline
Post 4hr
Control
EGF
1.4e+6
1.2e+6
1e+6
0.6e+5
0.2e+5
0.1e+5
p/s/cm²/sr

Figure 3

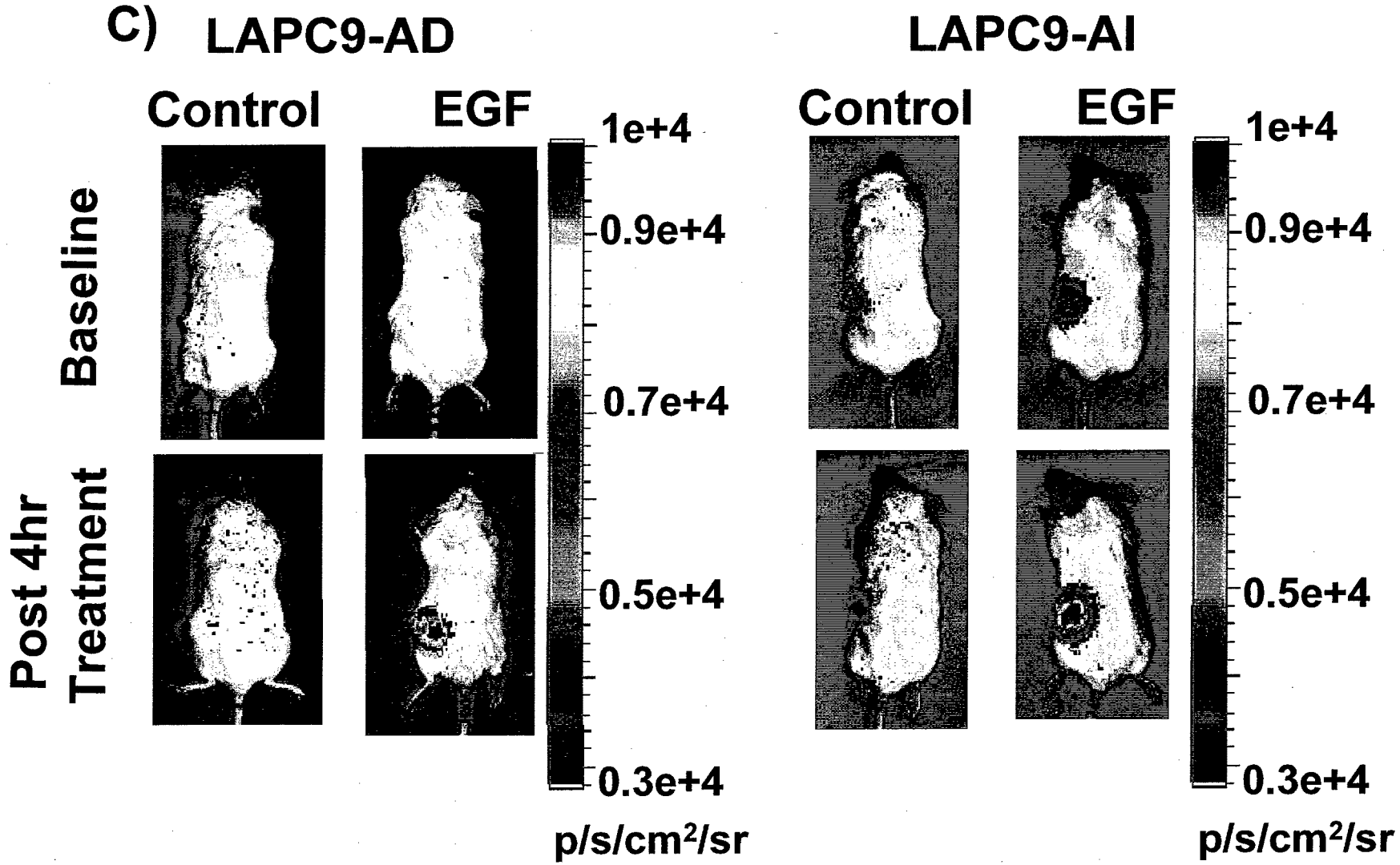
C)
LAPC9-AD
LAPC9-AI
Control
EGF
Control
EGF
Baseline
Post 4hr Treatment
1e+4
0.9e+4
0.7e+4
0.5e+4
0.3e+4
p/s/cm²/sr
1e+4
0.9e+4
0.7e+4
0.5e+4
0.3e+4
p/s/cm²/sr

Figure 3

D)

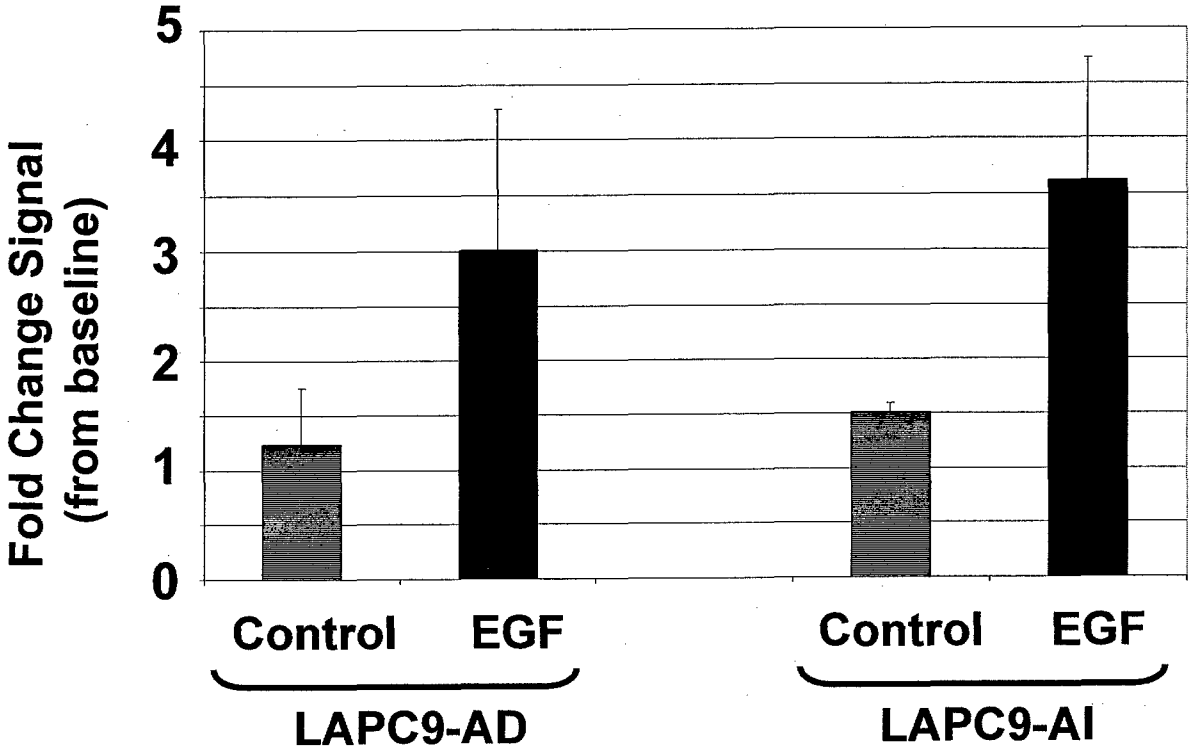
Fold Change Signal (from baseline)
5
4
3
2
1
0
Control
EGF
Control
EGF
LAPC9-AD
LAPC9-AI

Figure 4

A)

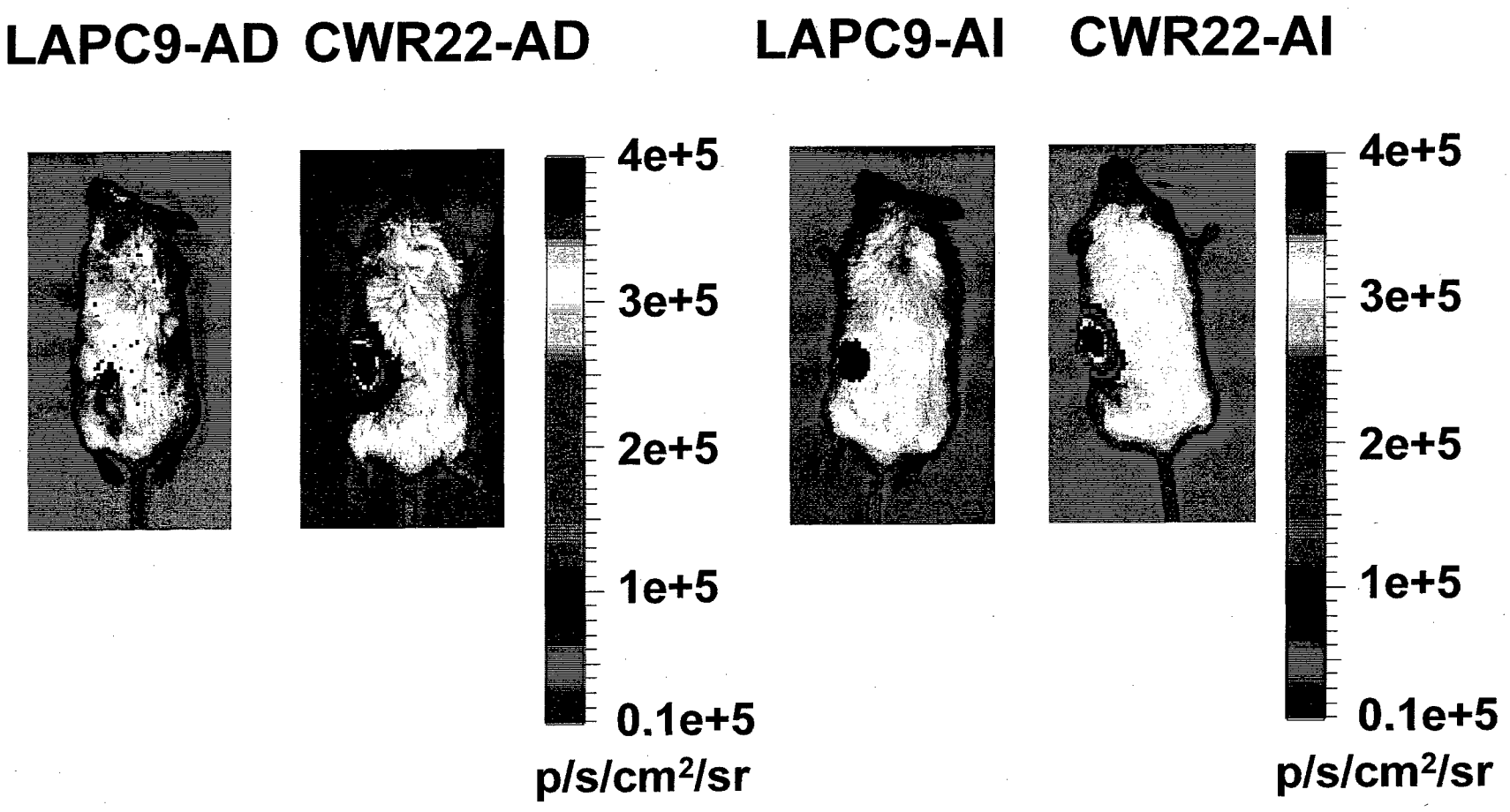
LAPC9-AD
CWR22-AD
LAPC9-AI
CWR22-AI
4e+5
3e+5
2e+5
1e+5
0.1e+5
p/s/cm²/sr
4e+5
3e+5
2e+5
1e+5
0.1e+5
p/s/cm²/sr

Figure 4

B)

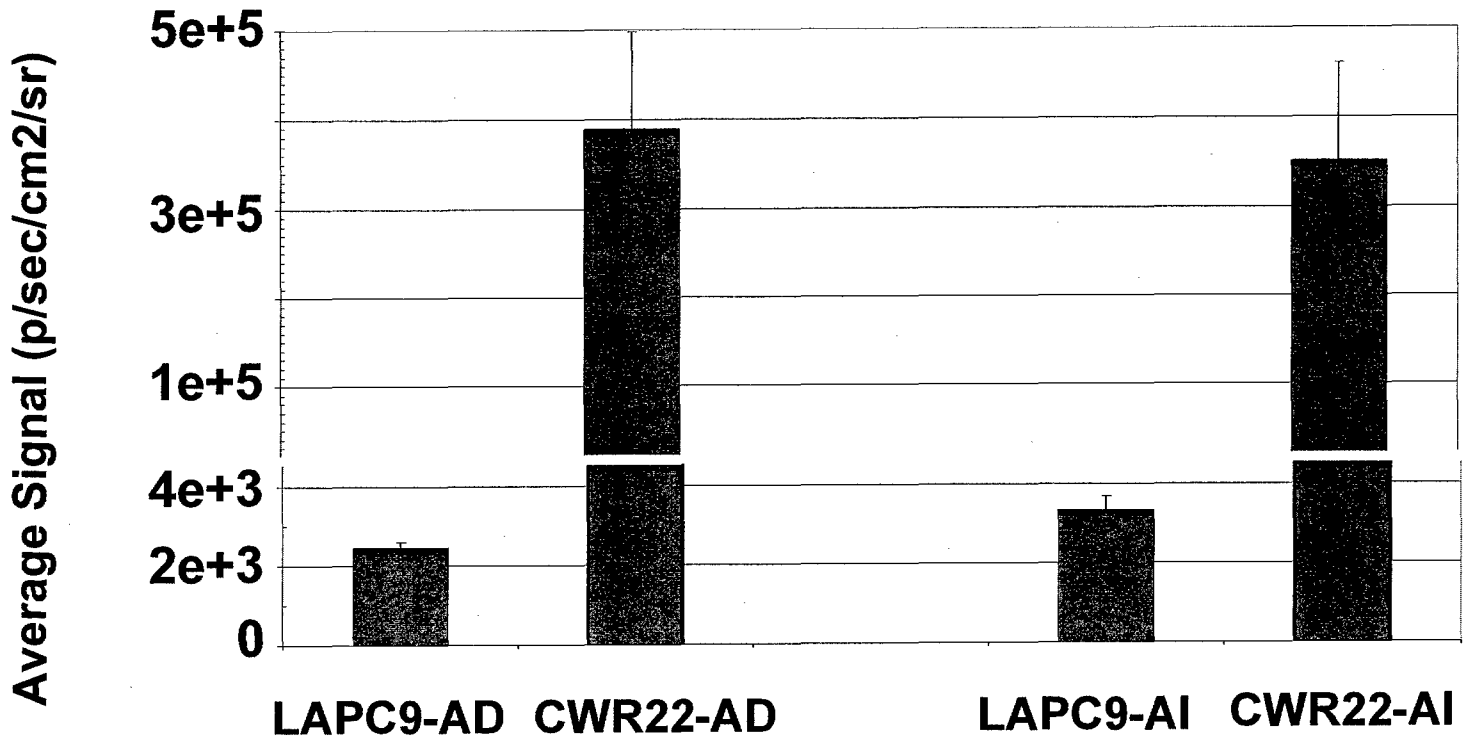
Average Signal (p/sec/cm2/sr)
5e+5
3e+5
1e+5
4e+3
2e+3
0
LAPC9-AD
CWR22-AD
LAPC9-AI
CWR22-AI

Figure 5

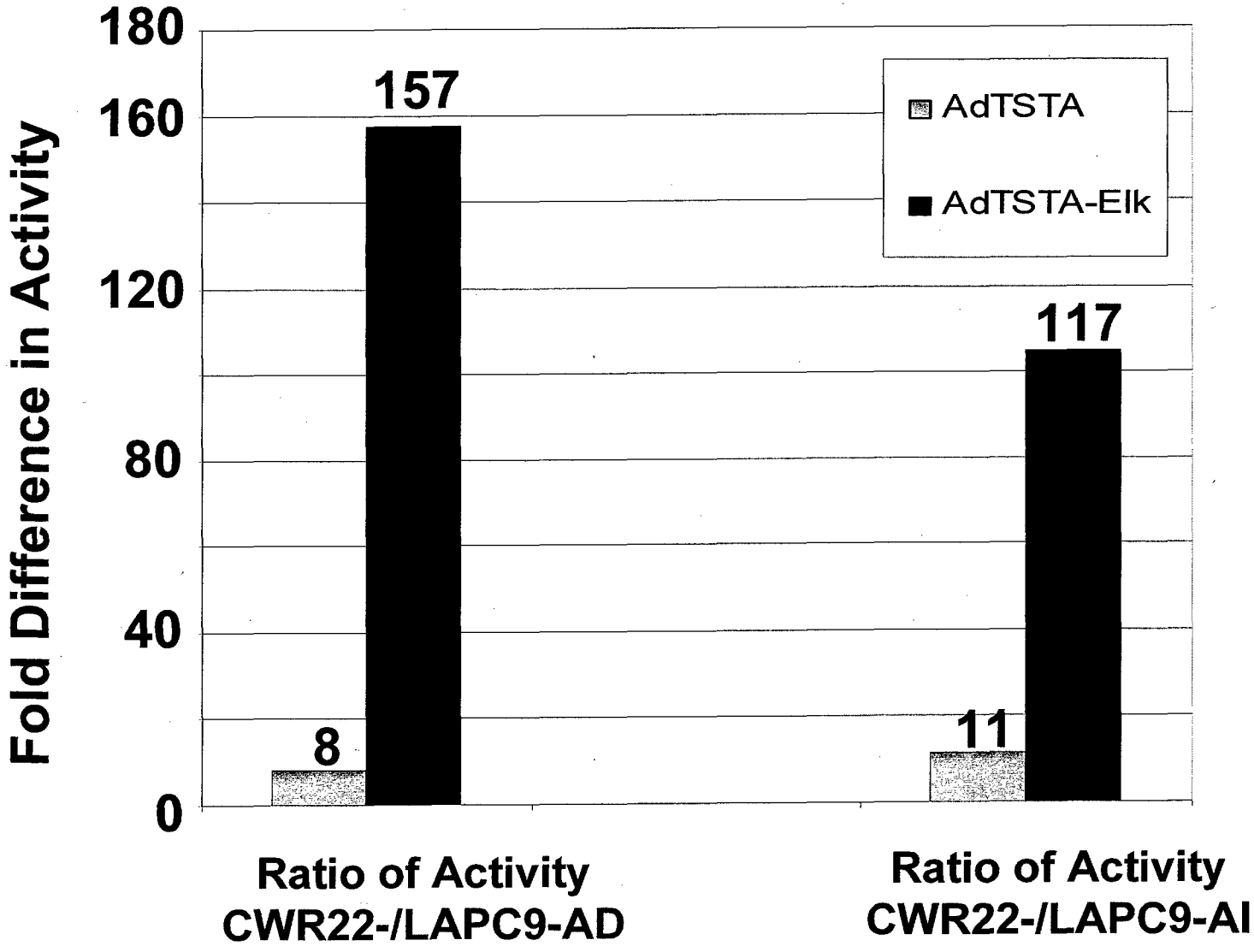
180
160
120
80
40
0
Fold Difference in Activity
157
8
117
11
AdTSTA
AdTSTA-Elk
Ratio of Activity
CWR22-/LAPC9-AD
Ratio of Activity
CWR22-/LAPC9-AI

Figure 6

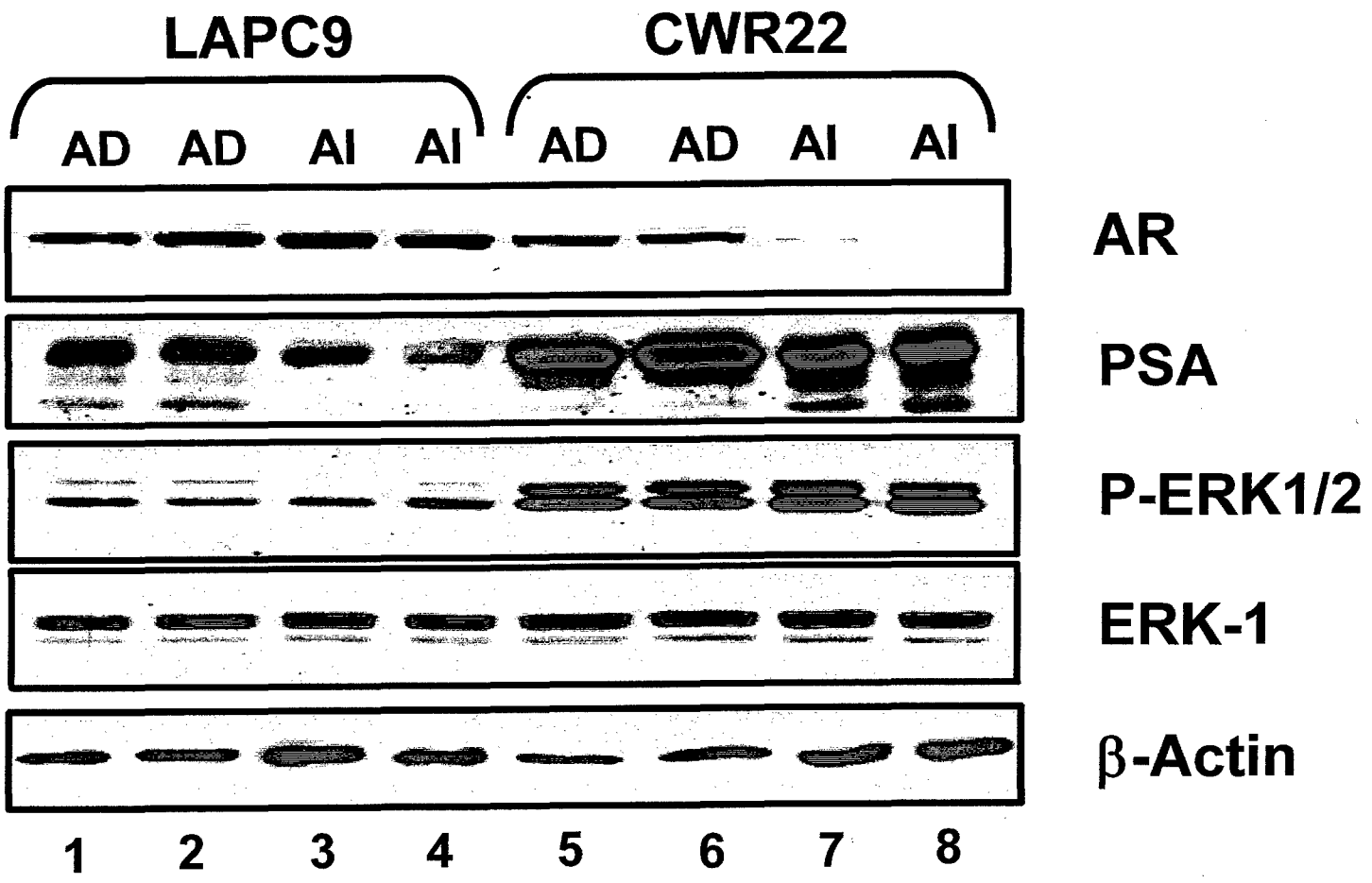
LAPC9
CWR22
AD AD AI AI AD AD AI AI
AR
PSA
P-ERK1/2
ERK-1
β-Actin
1 2 3 4 5 6 7 8